THE FLORIDA STATE UNIVERSITY

COLLEGE OF ARTS AND SCIENCES

MULTI- AND QUASI-DECADAL VARIATIONS OF SEA SURFACE
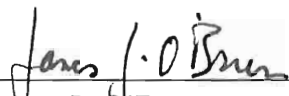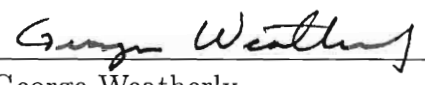TEMPERATURE ANOMALY IN THE NORTH ATLANIC

By

KEN-ICHI MIZOGUCHI

A Thesis submitted to the
Department of Oceanography
in partial fulfillment of the
requirements for the degree of
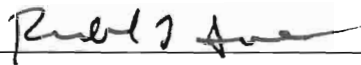Master of Science

Degree Awarded:
Fall Semester, 1997

The members of the Committee approve the thesis of KEN-ICHI
MIZOGUCHI defended on Nov 21, 1997.

James J. O'Brien
Professor Directing Thesis

Doron Nof
Committee Member

George Weatherly
Committee Member

Richard L. Iverson
Committee Member

ACKNOWLEDGEMENTS

I would like to thank my committee members, Dr.'s Nof, Weatherly, and Iverson, for their helpful comments regarding the contents of this thesis. I would also like to sincerely thank my major professor, Dr. O'Brien for his guidance, inspiration, tutelage, and most of all for allowing me the opportunity to perform this research. Special thanks to Dr. Steven Meyers for his advice and countless hours of help.

TABLE OF CONTENTS

LIST OF FIGURES

ABSTRACT

A 50-year propagating oscilation and 15-year rotating pattern are found in North Atlantic Ocean surface temperature anomaly. COADS sea surface temperature (SST) anomaly fields over the North Atlantic are investigated by means of propagating complex empirical orthogonal functions (CEOF) during the period of 1947 to 1992. Monthly anomaly time series for each $2°$ square from $20°$ N to $80°$ N and from $70°$ W to $30°$ E are low-pass filtered by 4 years. They are not detrended. The analysis is focused mainly on the first mode (Mode1) and the second and third modes combined (Mode2+3).

The first mode, representing 58% of the variance, indicates a basin-wide north-south pattern about $0.5°$C moving from off Newfoundland to southeastern Greenland, which coincides with the warming and cold events seen in previous studies. Slightly less than 1 cycle of this mode is found during the years of study, suggesting a roughly 50 year-oscillation.

The combined second and third modes, representing about 30% of the variance, is a cyclonic rotation within the subpolar gyre. It follows the subarctic gyre from the Labrador Sea to the northeast direction. This is a roughly 15 year-oscillation of $0.3°$C.

Windstress data with a four year low-pass filter are analyzed using Vector EOF (VEOF) analysis for comparison with SSTA. The first mode accounts for 43.2% of the total variance. The real part of the time function correlates to North Atlantic Oscillation (NAO) with the correlation coefficient as $r=0.79$. Time series of the SST anomaly of the combined mode in the Labrador Sea shows a high correlation to the first VEOF mode, indicating the variation is

coupled ocean-atmospheric mode.

Examination of windstress curl using real EOF analysis with no filtering also contains the NAO signal as $r=0.67$. The spectrum of the windstress curl is basically a white spectrum.

1. INTRODUCTION

In the North Atlantic the atmosphere commmunicates with deep oceanic wa-
ter masses at quasi- to multi-decadal timescales through convective overturning
(Talley, 1984). The ocean retains the long-term time scales of the atmosphere
due to the former's relatively large heat capacity and inertia. The ocean there-
fore provides a long-term memory for the global climate system. Sea surface
temperature (SST) anomaly is a useful indicator to use for understanding long-
term climate variability.

Low-frequency fluctuations in North Atlantic SST anomalies have been in-
vestigated in several studies. Kushnir (1994) partitioned SST anomalies into two
regimes of warm (1950-1964) and cold (1970-1984) events. Deser and Blackmon
(1993) examined the two major patterns of SST anomalies from real EOF anal-
ysis. The leading mode was characterized by a uniform polarity over the entire
basin with its largest value along the Gulf Stream, whereas the second had a
dipole pattern with anomalies of one sign east of Newfoundland and anomalies
of the opposite polarity off the southeast coast of the United States. After 1945
their results indicated about a 25 year period of fluctuation in SST anomaly in
their first mode, and a 10-15 year fluctuation in their second mode. They also
examined the linkage between SST anomalies and atmospheric circulations at
this period and found a significant correlation between the second EOF of SST
anomalies and the first EOF of air temperature anomalies. The latter is related
to the North Atlantic Oscillation (NAO).

The NAO has been found in atmospheric quantities such as air tempera-
ture and sea level pressure (SLP) (Cayan, 1992a; Barnston, 1987; Wallace and

1

Gützler, 1981). Rogers and Loon (1978) and Rogers and Loon (1979) have described the fluctuations in winter air temperature associated with the NAO. Wallace and Gützler (1981) used real EOF analysis of 500 mb height fields to classify the atmospheric teleconnection into four modes, the largest of which was the NAO.

The NAO signal in SLP anomaly is a standing oscillation extending over the entire North Atlantic. The NAO index (from the Climate Prediction Center) is the difference of normalized sea level pressures between Lisbon, Portugal and Stykkisholmur, Iceland (Fig. 1). In the positive phase of the NAO, westerlies across the North Atlantic strengthen due to the deepening of the Icelandic low and the strengthening of the Atlantic high located around 40°N in the mid-Atlantic. The westerly winds blow over warm Gulf Stream waters delivering mild air to Europe, while the cold air over the Icelandic low is advected over the Greenland-Labrador area due to the deepening of the Icelandic low.

The NAO signal has been found in several studies of North Atlantic SST anomaly. Bjerknes (1964), Deser and Blackmon (1993) and Kushnir (1994) investigated the relationship between observed SLP and SST anomaly. At interannual to decadal time scales, oceanic variability was found to be forced by atmospheric variability. However, at multi-decadal time scales they concluded that the ocean drives atmospheric changes. Molinari et al. (1997) analyzed the low-pass filtered and detrended subsurface temperature fields of the western Atlantic in the upper 400-m and found that the temperature variations in the time series corresponded to the NAO index.

Houghton (1996) described the quasi-decadal fluctuations of subsurface tem-

perature and salinity in the Labrador Sea and found the variability at this time scale can penetrate to the same depth as the seasonal cycle in both the subtropical and subpolar gyres. He suggested that in the western subpolar gyre, quasi-decadal fluctuations of the subsurface temperature are affected by the modulation of the wind stress through precipitation, river runoff and ice melt over this region.

Ice melt from the Arctic is believed to play a role in the formation of the "Great Salinity Anomaly" (GSA) (Dickson et al., 1988). The GSA is characterized as large, near-surface fresher water that appeared east of Greenland in the late 1960s. It was carried around Greenland by the East and West Greenland Currents, passing along the Labrador Sea on the Labrador Currents, and was advected by the North Atlantic Currents around the cyclonic subpolar gyre. It was recognized again off Newfoundland in 1971-72 and was slowly carried to Europe in the North Atlantic Curent back to its origin in 1981-82. The entire cycle took a little over 14 years to complete. The overall propagation speed around the subpolar gyre is roughly estimated at $3cms^{-1}$.

The GSA greatly impacted the deep convection in the Atlantic Ocean. Normally, where deep convection occurs in the north Atlantic, the surface water sinks and mixes with the deeper water due to the strong winter cooling. However, when the GSA passed over this region, it stabilized the water column, preventing the cold surface water from convecting into the deeper waters.

Häkkinen (1993) simulated the GSA event using a fully prognostic Arctic ice-ocean model during the period of 1955-1975. The model was forced using daily winds during that period. The model results showed the origin of the GSA

was due to freshwater excess that resulted from greater than normal ice export in the Arctic.

Reverdin et al. (1997) investigated the variability of the North Atlantic sub-arctic gyre by performing an EOF analysis on temperature and salinity at different stations and found a propagating signal from the west to the northeast in the subarctic gyre. This propagation was considered to result from fresh water originating in the Labrador Sea being advected to the northeast. Hansen and Bezdek (1996) (HB) showed a propagating feature in a 4-year low-pass filtered and detrended SST anomaly along the subarctic and subtropical gyres in the North Atlantic at decadal time scales.

Weaver and Sarachik (1991) described numerical experiments that exhibited decadal oscillations under steady forcing. The salinity and temperature anomalies were advected inbetween the subtropical and subpolar gyres eastward and poleward. The speed of the propagation was estimated as the order 1 to 2 km d^{-1} (1.2 to 2.3 (cm/s)).

Grötzner et al. (1996) derived a climate cycle of about 17 years from a global coupled ocean-atmosphere circulation model, whereas a similar analysis of corresponding observations indicated a period of about 12 years. They speculated that the advection of temperature anomalies due to mean currents might have some influence on this oscillation in the North Atlantic.

Many of the studies analyzing SST anomaly data, including those mentioned above, have been done with the technique of conventional real EOF analysis, which decomposes the data fields into real orthogonal pairs of spatial and temporal patterns. The product of the resulting time functions (TF) and spatial

4

functions (SF) reproduces the major patterns of the analyzed data sets. However, the shortcoming of the EOF is that it tends to capture only the stationary patterns. That is, the extracted patterns are spatially fixed.

As described above, SST and subsurface salinity anomalies in the subpolar North Atlantic have propagating features. Therefore, it is necessary to understand the spatio-temporal evolution of SST anomaly field at the decadal time scales. Latif and Barnet (1994) investigated the characteristic evolution of the integrated upper 500m heat content in the Pacific Ocean from a coupled model of global ocean-atmosphere general circulation (ECHO), by using complex EOF analysis (CEOF) with a 3 year low-pass filter. They found that the leading mode of CEOF had a period of 20 years and that the reconstructed field has the spatial evolution in time. Studies using CEOF in other applications include (Barnett, 1983; Horel, 1984; Shriver et al., 1991; Sharp, 1996).

In this paper the investigation mainly focuses on the SST anomaly in the subpolar gyre at quasi- and multi-decadal time scales. The monthly SST anomaly (SSTA) is defined as the departure from the monthly climatology. The mathematical method to analyze the data set is CEOFs. Surface wind stress is also studied using Vector EOF (VEOF) (Legler, 1983; Servain and Legler, 1986; Breidenbach, 1990). Both data sets are from Comprehensive Ocean-Atmosphere Data Set (COADS) covering the North Atlantic 20° N northward. Windstress and climatology of surface ocean current over the domain are used to compute the zonal advective speed for comparison with the results from SSTA CEOF. The climatology of 10 m model currents are provided by S. Häkkinen and Ekman currents (Fig. 2) are calculated from the climatology of the windstress. The

data are described in section 2, the method in section 3. The results are shown
and discussed in the context of other observations and other model results in
section 4. The summary and conclusion are in section 5.

2. DATA

A 42 year subset of COADS (Woodruff et al., 1987) monthly sea surface temperature (SST) covering the North Atlantic from 70° W to 30° E and from 20° N to 80° N from 1947 through 1992 with a resolution of $2° \times 2°$ is examined. COADS has inherent uncertaintities due to historical changes in instrumentation, observation techniques, coding methods, data density and ship tracking. The historical data sets after 1947 were chosen due to their high spatial coverage. This is also after the large shift in SST anomaly observed by Deser and Blackmon (1993). The same data processing now described for the SST is also applied to the zonal and meridional component of wind stress data set from 1947 through 1992. The Mediterranean Sea and Baltic Sea are ignored for this analysis.

The monthly climatology fields of SST is calculated by averaging all the months in time at each location. In the early years of the time series, there is a lack of data in the North Atlantic from 60° N to 80° N and in the Labrador Sea due to severe weather conditions and ice coverage. The area off the African continent from 30° W to 20° W and from 20° N to 30° N lack data in late 1940s and 1950s regardless of the seasons (Fig. 3). The area from 60° N to 80° N of the historical data set is replaced by the climatology when there is a missing value. Missing values in other regions are filled by interpolating from surrouding data values. Each month of the SSTA and the 46 year time series of SST at each location then has an E-W-E and a N-S-N 1-2-1 Hanning filter applied three times. A new climatology is calculated from the filled, interpolated and smoothed fields and the original climatology is discarded. The data used in the

calculation are the differences from the new climatology.

In January, all the isotherms are positive and run roughly east-west (Fig. 4). The gradient of the isotherms is strongest off Newfoundland at 55° W and 45° N where the Gulf Stream flows. The minimum and maximum values are 2° C and 24° C, near the northern and southern boundaries, respectively. In April two negative temperature regions appear near the northern boundary of the ocean domain. One is located northeast of Iceland at 10° W and 75° N, and, the other is the northern part of Labrador Strait at 60° W and 70° N. The two cold fronts push the 2° C lines southwards while isotherms $\geq 6°C$ remain essentially unchanged. In July the 2° C line invades all the way to 80° N and to the north of Labrador Sea. In the south of the domain 28° C line moves to the north. The temperatures of the Gulf Stream are warmer and its temperature gradient relaxes compared to the winter distribution. In October the temperature field starts to go back to its winter distribution.

The domain is on a 51×31 grid, where there are 950 spatial points in the ocean and 631 land points set. The monthly anomaly time series at each ocean point are low-pass filtered using a four year running-mean. The time series of anomalies are not detrended. As will be shown below, the low-pass filtered SSTA has a very slow variation which would be suppressed by linear-detrending.

3. METHOD

two dimensional propagating complex orthogonal function (CEOF)

Two dimensional propagating complex empirical orthogonal function analysis (CEOF) is used in this study to extract physical information on propagating features from the SSTA at climatic time scales.

A one dimensional spatial array, $u(x_m, t)$, is formed from the two dimensional SST anomaly field $u(x_m, t) = \text{SST}(\mathbf{r}_m, t)$, where $\mathbf{r}_m$ is the position vector and t is the time index.

$$u(x_m, t) = \sum_{\omega} [a_m(\omega)cos(\omega t) + b_m sin(\omega t)] \tag{1}$$

where $a_m(\omega)$, $b_m(\omega)$ are the Fourier coefficients.

Define the complex representation of a variable as

$$U_m = \sum_{\omega} c_m(\omega) e^{-i\omega t} \tag{2}$$

where $c_m(\omega) = a_m(\omega) + i b_m(\omega)$

The expansion of (2) gives

$$U_m(t) = \sum_{\omega} \{[a_m(\omega)cos(\omega t) + b_m(\omega)sin(\omega t)] + i[b_m(\omega)cos(\omega t) - a_m(\omega)sin(\omega t)]\}$$
$$= u_m(t) + i\hat{u}_m(t) \tag{3}$$

The imaginary part $\hat{u}_m(t)$ is the Hilbert transform of the real part, which is in fact a $\pi/2$ shifted function of the real part in time with the same magnitude of the Fourier transform. Here u_m is the SSTA.

A complex-valued spatio-temporal matrix $U_{m,t}$ is formed in such a way that each row of the matrix is a temporal array, and each column is a spatial array,

9

where $m = 1, 2, ..., M$, $t = 1, 2, ..., N$, and $M = 950$ (ocean points), $N = 504$ (months). The covariance array is calculated by multiplying the $M \times N$ matrix by its transpose to form a $N \times N$ Hermitian matrix which is symmetric with real-valued diagonal elements. By solving the eigensystem equation of the covariance matrix, the eigenvalue vector λ_i, where $i = 1, 2, ...N$, and the spatial and temporal functions (eigenvectors) are obtained. Normalized eigenvalues represent a relative variance of the original data set $(\frac{\lambda_i}{\sum_{i=1}^{n} \lambda_i})$.

The data $U_m(t)$ are reconstructed by the summation of spatial (SF) and temporal functions (TF) as follows:

$$U_m(t) = \sum_l [S_l(m)e^{i\theta_l(m)}]^* [R_l(t)e^{i\phi_l(t)}] \tag{4}$$

where $SF = S_l(m)e^{i\theta_l(m)}$ and $TF = R_l(t)e^{i\phi_l(t)}$, respectively and $*$ denotes the complex conjugate.

The spatial amplitude function $S_l(m)$ is defined as

$$S_l(m) = [(SF)(SF)^*]^{1/2} \tag{5}$$

The spatial phase function $\theta_l(m)$

$$\theta_l(m) = \arctan[Im(SF)/Re(SF)] \tag{6}$$

The wave number **k** is obtained by

$$\mathbf{k} = \frac{\partial \theta_l(m)}{\partial \mathbf{x}} \tag{7}$$

, where $\mathbf{x} = (x, y)$

The temporal amplitude function $R_l(t)$

$$R_l(t) = [(TF)(TF)^*]^{1/2} \tag{8}$$

10

10

The temporal phase function $\phi_l(t)$

$$\phi_l(t) = \arctan[Im(TF)/Re(TF)] \tag{9}$$

The frequency ω is calculated from the temporal phase function as

$$\omega = \frac{\partial \phi_l(t)}{\partial t} \tag{10}$$

Vector EOF (VEOF)

Vector EOF analysis is performed for the zonal and the meridional component of the wind stress anomalies. These replace the real and the imaginary part of the complex values $U_{m,t}$, respectively. The mathematical derivation is in principle the same as the CEOF with the exception of the replacement of the two components. The original data are reconstructed by the summation of the resulting complex-valued spatial (A_l) and temporal (X_l) functions. Resulting complex-valued eigenvectors are written as

$$U_m(t) = \sum_l A_l X_l \tag{11}$$

When displaying the spatial function it is necessary to add an arbitrary rotation angle to each of the wind stress vectors to make the wind fields recognizable patterns because eigenvectors contain an arbitrary phase. The same angle should be subtracted from the associated time eigenvectors. The complex-valued vector can also be written as

$$U_m(t) = \sum_l A_l e^{i\theta} X_l e^{-i\theta} \tag{12}$$

In this paper, each vector of the first spatial mode is not rotated ($\theta = 0°$).

11

The temporal eigenvectors are complex-valued with the combination of real (X_r) and imaginary (X_i) components. To calculate the evolution of the spatial fields the magnitude of each of the spatial EOFs must be multiplied by the magnitude $(\sqrt{X_r^2 + X_i^2})$ of the time EOFs and the angle of the time eigenvector rotated by $\arctan(X_i/X_r)$. The magnitude of the temporal function controls the strength of the winds and the phase of temporal function controls the direction of the winds.

climatology of ocean current

The climatology of 10 m model currents (provided by S. Häkkinen) and Ekman currents (Fig. 2) calculated from the climatology of the windstress described above are used to estimate the advective speeds in the North Atlantic. The Ekman currents calculated from the windstress are simply added to the 10 m currents. The total current is then $\mathbf{u} = \mathbf{u}_{10} + \mathbf{u}_{Ek}$, where $\mathbf{u}_{Ek}$ is the linear Ekman current velocity vector. These are compared to the propagation speed of the SSTA. The model currents are from a fully prognostic coupled ocean-ice model (Mauritzen and Häkkinen (1997)) with the resolution of 7/10 in longitude and 9/10 in latitude. They are averaged spatially into $2° \times 2°$ boxes. The domain is the same as that of SSTA and windstress.

12

4. RESULTS AND DISCUSSION

The first 3 modes of SSTA CEOF account for more than 87.0 % of the total variance, of which the first mode accounts for 58.3%, the second and the third 16.1% and 12.7%, respectively. The first 3 modes appear to be distinctively above the noise level (Fig. 5 (a)) and, therefore, have some physical meaning. Only the first three modes are discussed hereafter.

4.1 CEOF Mode 1

spatial properties

The spatial amplitude function for CEOF1 (Fig. 17(a)) contains a double-peaked pattern found off Newfoundland. This is the region where the largest warm anomalies appear in the reconstructed SSTA (Fig. 6) in the early 1950s and the cold anomalies appear in the mid-1970s.

The spatial phase from 50°N to 70°N, where deep water formation occurs, is highlighted in Fig. 18(a). The phase in this region increases in a nearly linear fashion to the north, indicating nearly steady northward propagation of SST anomalies.

temporal properties

Both the real and imaginary parts of the time series (Fig. 33(a)) show slow variability that does not finish a single cycle. A half-cycle occurs approximately from about 1950 to 1970, which is when the warm event occured from Newfoundland to southeast of Greenland (Fig. 6).

The temporal phase function of mode 1 is shown in Fig. 19(a). Since the argument of the phase function is defined from 0° to 360° the time series of the

13

function cannot be plotted as a continuous function. Therefore, it is defined from $0°$ to $1500°$ to make it continuous Fig. 20(a). The y intersept has the value of $332.7°$. The linear-fit is applied to this function so that the fundamental period ω is estimated. The period of the mode 1 is about 43.7 years, which is about twice longer than the half period of about 21 years estimated from the series in Fig. 33(a).

Often, the meriodional speed of propagation for each mode can be calculated as $c = \omega/l$, where ω is the frequency in (10) and l is the meridional wave number. The frequency ω can be reasonably estimated as a constant, but the wave number l is not constant in space, so the phase speed varies with geographic location.

Reconstructed SST anomaly (SSTA)

As shown by (4), the time evolution of the spatial field of each mode is obtained by multiplying the spatial and temporal function of that mode and taking the real component. The reconstructed spatial patterns for SSTA for CEOF1 are shown in Fig. 6. Several years of variation are represented by each month due to the 4 year low-pass filtering. Following Hansen and Bezdek (1996), January is chosen as the representative month of each year. The 42 years of January temperature anomalies are shown in Fig. 6. On January 1949, a warm anomaly is located off Newfoundland at around $60°$ W and $45°$ N.

Contemporaneous with the warm anomaly is the cold anomaly south off Greenland at around $35°$ W and $60°$ N. As the warm anomaly grows the cold anomaly weakens and slowly dissipates. By 1953 most of the ocean mid-basin from $20°$ N to $70°$ N is covered with the warm anomaly. After 1954 this anomaly

14

reduces its size and migrates northward, until eventually it disappears at around 60° W and 45° N in 1973, the same location where the cold anomaly disappeared in 1951.

In 1958 a new premonitory cold event appears off New York at around 70° W and 40° N while the opposite anomaly occurs to the north. During 1967-68 another cold patch emerges from the eastern side of the basin off the African continent, merging with the one from the west. As the cold anomaly strengthens it follows the same path of the preceding warm event, and the warm event weakens and disappears south of Greenland. In 1985 another warm anomaly appears off New York and begins to follow the same path until 1990, the end of the time series. Over the course of entire 42 years, only the warm event completes nearly one cycle. Rough estimation of the warm anomaly speed is about 0.3 km d^{-1} (0.35 cm/s) assuming the distance that the warm anomaly travels and the duration that it survives are 20° (from 40° N to 60° N) and 21 years (from 1953 to 1973), respectively.

multi-decadal change

Multi-decadal variability in North Atlantic SSTA is clearly seen in zonally averaged bands (Fig. 34). The timing of these variations change with latitude. Warming begins before 1950 and lasts until around 1964, the beginning of the cold event that lasts until around 1985. The timing of these events agrees with those found in Kushnir (1994). The transition from warm to cold anomalies is also seen in a time-latitude presentation of zonally-averaged SSTA (Fig. 35), in which the two clearly recognized temperature events become delineated. These features exhibit a northward propagation.

15

The difference field between the warm interval (1950 to 1964) and the cold interval (1970 to 1984) are calculated (Fig. 17 (d)). The pattern that comes out from the subtraction is similar to the spatial amplitude function Fig. 17(a). Only one strong warm patch is situated at 45° W and 50° N. A similar analysis by Kushnir (1994) shows the three temperature extrema occurring along the northern boundary of the domain, around Iceland and in the Labrador Sea. The cold patch in Kushnir (1994) is substituted by a warm anomaly in Fig. 17(d). The warm anomalies in his analysis are similar to those in this analysis. The result in Fig. 17(d) is also very similar to SST changes found by Delworth et al. (1993) (their Fig. 6(a)) associated with a 40-50 year periodicity in the thermohaline circulation (THC) of a fully coupled ocean-atmosphere model. The oscillation seemed to be driven by density anomalies in the region of deep water formation (52° N to 72° N).

HB showed a propagating SSTA following the subpolar gyre, with a SSTA that was warm overall in the 1950s and 1960s. In the late 1960s, a cold SSTA developed near 40° N, propagated into the subpolar gyre, had its maximam extent in the mid 1970s, weakened around 1980 and reestablishes in the mid 1980s. The overall timing of warm and cold SSTA is conincidental with that of HB. However, in our analysis, the SSTA propagating feature of CEOF1 does not follow the subpolar gyre but continuously propagates northward. This difference may be due to the detrending of the SSTA in the HB analysis, which removed much of the long-term variations found in CEOF1, leaving mostly the quasi-decadal features found in higher CEOF modes described below.

16

4.2 CEOF Mode 2 and Mode 3

The second and third modes have comparable variance of 16.1% and 12.7%, respectively. These modes are first examined separately, then in combination as a rotating mode.

spatial properties

The spatial amplitude of mode 2 has a maximum region located off Newfoundland (Fig. 17(b)). Three secondary maxima are found, two on either side of the southern tip of Greenland, and one north of Iceland. The spatial phase (Fig. 18(b)) indicates propagation from the north of the Labrador Strait around $70°$ N. The anomalies propagate from the north of Labrador Strait southeastwards to the center of the basin at $35°$ W, $45°$ N, turn eastward beneath the phase nexus at $55°$ N and $30°$ W, and divert to the north, up to $70°$ N northeast of Iceland. This phase structure suggests the presence of a phenomenon rotating about the subpolar gyre, but the direction of rotation can only be determined in conjunction with the temporal phase, described below.

For mode 3 the spatial amplitude (Fig. 17(c)) has a strong maximum located northeast of Newfoundland at the entrance of Labrador Strait. Also, there is another small maximum south of Iceland and another east of Iceland east of Europe. The corresponding spatial phase (Fig. 18(c)) also seems to suggest that the SST anomalies propagate southeastward from the Labrador Strait into the Atlantic basin, and turn eastwards towards England. Following this path, the phase increases in a nearly linear fashion. A phase nexus is found near the same location as for mode 2, suggesting the two modes are dynamically related.

temporal properties

17

The real part of the temporal function for mode 2 (Fig. 33(b)) shows a sinosoidal behavior, especially after 1967, with a period of around 15 years. The temporal phase in Fig. 19(b) suggests a varying period, based on the time between peak values, between 12 and 18 years. A least squares linear fit to the phase function (Fig. 20(b)) produces an average period of 14.4 years. The increasing phase of this temporal mode, coupled with the phase of the spatial mode, indicates cyclonic propagation about the subpolar gyre.

The temporal phase function for mode 3 (Fig. 19(c)) is similar to that of mode 2, though the former is relatively jagged with a burst of 1-2 year variations in the early 1970s. The linear fit to the temporal phase yields a period of 13.9 years. The nearly constant slope of the temporal phase (Fig. 20(c)) has important implications for the speed of propagating features in mode 3. In conjunction with the spatial phase the temporal phase indicates roughly steady movement out of the Labrador Sea into the Atlantic and eastward towards Europe.

During the burst of short-term fluctuations in the 1970s, the average reconstructed SST anomaly due to mode 3 dissapears suddenly (not shown). Deser and Blackmon (1993) noticed a shift in atmospheric circulation around 1971 that increased the intensity of winds and evaporative heat flux. This abrupt shift in mode 3 SSTA might be related to the shift of the atmospheric circulation.

The similarity between mode 2 and mode 3 in their relative variance, spatial structure and temporal phase suggests these two modes represent a single split mode. In the following subsection we will discuss the combination of CEOF mode 2 and mode 3. Sharp (1996) discussed using CEOF analysis applied to

18

a field that has a rotating feature. CEOF analysis treats this case in a similar fashion to the way a real EOF would split a linearly propagating feature. In CEOFs, circular motion splits into two equal variance modes. Combination of the two modes reconstitutes the rotating structure.

4.3 CEOF Mode 2+3

Reconstructed SSTA

The real part of the sum of modes 2 and 3 is now examined. January maps of the anomalies are examined (Fig. 22) from 1949 through 1990. In 1950 a cold anomaly is situated in the mid-basin around $25°$ W, $50°$ N and a weak cold anomaly is developing north of Iceland. A warm anomaly is at the entrance of the Labrador Sea (LS) at $50°$ W, $60°$ N and another east of Scandinavia. This alternating pattern of warm and cold anomalies travels around the subpolar gyre cyclonically. The center of the circular motion is located roughly inbetween Greenland and Iceland.

By 1955 the warm anomaly originally off Newfoundland has replaced the cold anomaly. The warm anomaly is now found in the mid-basin and the cold anomaly now straddles the east and the west of southern Greenland. These features continue to travel about the gyre, until the initial position of the warm and the cold anomalies is reestablished in 1965. The 1950 pattern does not recur as expected around 1978, though a warm anomaly does exist off Labrador a cold anomaly is not present in the mid-basin. In 1971 the 1955 pattern re-establishes, occuring again in 1983. The alternating anomalies seem to be advected by the currents in the North Atlantic, one of which is the North Atlantic Current that parallels the $50°$ N line.

19

The speeds of warm and cold anomalies are both estimated as 1.3 cm/s. The warm and cold anomalies are followed from 1951 to 1958 and from 1959 to 1966, respectively. They propagate from 50° W to 20° W during this period of eight years. These anomalies are selected because their propagation is distinctively stronger than during any other years. The propagation speed estimated for the warm and cold anomalies is comparable to that from Weaver and Sarachik (1991) (their speed was about 1.2 to 2.3 cm/s). HB estimated the propagation speed of SSTA using autocorrelation analysis as 2.3 cm/s.

Grötzner et al. (1996) speculated that the decadal oscillation in the North Atlantic is attributed to the advection of temperature anomalies carried by the mean current. The mean speed of surface ocean current derived from the combined climatology of model extracted and Ekman current (Fig. 2) is roughly 10 cm/s. This is almost 10 times bigger than that from CEOF mode2+3.

This combined mode has a large impact on the Labrador Sea (LS). SSTA from CEOF mode2+3 are averaged over the region from 48° N to 60° N and 60° W to 60° W. This is compared to the SSTA averaged over the area along the Labrador-Newfoundland continental margin from 48° N to 60° N seaward from Houghton (1996) (his Fig. 1) in Fig. 37. His time series was produced from January–March monthly anomalies calculated by subtracting the climatological mean. For this comparison his result is detrended and both timeseries are normalized by twice their respective standard deviation. The period and relative amplitude of oscillation are nearly identical in both the time series. Houghton (1996) suggested these fluctuations might be related to latent heat flux and surface fresh water anomalies due to local precipitation, river runoff and ice

20

melt, which are subject to modulation by variations in the anomalous wind stress. This is supported by the results of VEOF analysis of the windstress.

The above timeseries of SSTA and the real part of the time series of the first mode VEOF are correlated after 1960 and before 1987 (Fig. 36). The first temporal VEOF function is dominated by its real part, which has a standard deviation 4.6 times larger than the imaginary part. The first mode wind field changes amplitude mostly in response to changes in the real part of the temporal function, so neglecting the imaginary component in this analysis is not unreasonable. This is consistent with the notion that the NAO is a standing pattern of high and low pressure. Reversal of the NAO pattern implies reversal of the winds. The real part of the first VEOF is correlated with the NAO signal (Fig. 1), $r=0.79$ at zero lag. The imaginary component does not correlate to the NAO, $r=0.05$ at zero lag. The physical contribution of the imaginary component is largely to rotate the vectors through their reversals.

A relationship between wind/NAO and SST anomalies was also found by Deser and Blackmon (1993). They showed the wind anomaly patterns regressed onto the temporal function of EOF 2 of SSTA resembled the wind anomalies of the NAO in positive phase (their Fig. 4). It was shown that when SSTA between 50° N and 60° N in the mid-Atlantic are colder than normal, the near-surface westerly winds are stronger than normal. It was speculated that stronger winds cool the ocean surface by enhancing evaporation. (Cayan, 1992b) showed that latent heat flux anomalies have a spatial pattern similar to that of the NAO SLP pattern. These have been roughly correlated since 1960 at the quasi-decadal time scales.

21

5. SUMMARY AND CONCLUSION

The multi- and quasi-decadal variabilities of the sea surface temperature (SST) anomaly over the North Atlantic are investigated by means of two dimensional propagating CEOF. 42 years of COADS SST and wind stress data sets from 1947 to 1992 are used. After removing monthly climatology and four year low-pass filtering the SST anomaly (SSTA) and windstress anomaly are submitted to CEOF and VEOF, respectivly. We assume that the first 3 modes are physically significant. The analysis is focused mainly on first CEOF (mode1) and the combined second and third modes (mode2+3). The variance of the three modes accounts for 87.0% of the total variance.

The results of this study indicate that SSTA has two different time scales of multi- and quasi-decadal fluctuations represented by mode1 and mode2+3, repectively. Mode1 is a very slow oscillation with a 50 year period. The mode2+3 is a quasi-decadal fluctuation with a 15 year period. The former has spatial evolution that is basin-wide, with alternate warm and cold anomalies appearing off Newfoundland and migrating northward until they disappear south of Greenland. It is important to notice that the centers of action of the two modes both occur in the vicinity of the Labrador Sea, Newfoundland and south of Greenland where there is Deep Water formation taking place.

Bjerknes (1964) suggested that multi-decadal changes in SSTA over the northern North Atlantic are associated with variations in the intensity of the THC. Mode1 is a new representation of these low-frquency changes in SSTA and therefore should be linked to the varations in THC.

Mode2+3 contains quasi-decadal time scales with alternate warm and cold

22

anomalies propagating from the Labrador Sea eastwards following the subpolar gyre, suggestive of the Great Salinity Anomaly (GSA) (Dickson et al., 1988) and Lesser Great Salinity Anomaly (LGSA) (Lozier et al., 1995). The propagation speed of mode2+3 is estimated approximately as 1.3 cm/s, comparable with the speed of salinity and temperature anomalies in a numerical experiment of Weaver and Sarachik (1991). In their experiement it is suggested that the propagation of the anomalies are attributed to the advection of currents in the North Atlantic.

The source of fresh water release in the Labrador Sea is strongly related to the wind stress modulation of the North Atlantic Oscillation (NAO) over that area at quasi-decadal time scales. The first mode of VEOFs of the wind-stress, which accounts for 43.2 % of the total variance, correlates to NAO index (r=0.79). The change of the wind seems not to have the direct impact on SSTA but indirect impact through other quantities such as precipitation, river runoff and ice melt (Houghton, 1996).

The low-salinity anomaly of the GSA event appeared at around 25° W, 65° N in 1968 off east Greenland and travelled southward, carried by the Greenland Currents to be found in the LS at around 43° W, 68° N in 1969-1970 (schematic in Schmitt (1996)). This water hovered off Newfoundland at 45° W, 48° N in 1971-1972. It was slowly advected by the North Atlantic Current and was found at 32° W, 48° N in 1974. The North Atlantic Current carried it over to north of England by 1976. Afterwards, a branch of the North Atlantic Current called Norwegian Current transfers it back to its orgin in 1979. The orgin of GSA is thought to lie in a large discharge of ice from the Arctic Ocean in 1967. It took

the anomaly 14 years to complete one cycle of the event. Lozier et al. (1995) found another less saline anomaly arrived at the LS in 1978 - 1984. Belkin et al. (1996) have noticed that this low salinity anomaly took a similar path as the previous GSA in 1971. It arrived in the northern LS in 1982, and departed southwards by 1984.

There appears to be a correspondence between the low salinity anomalies and the cold anomalies. In 1968, when a GSA first appeared east of the Greenland, a cold anomaly exists around Iceland (Fig. 22). In 1969-70, a cold anomaly straddles east and west of the Greenland tip when the GSA arrived in the LS. A warm anomaly is situated off Newfoundland at 50° W, 50° N. The cold patch reaches its maximum amplitude in 1971-1972. The arrival of LGSA is not marked in the SSTA of the LS in 1982, however, by 1983 the LS is occupied by the cold anomaly. The cold anomaly advects to the south and east following the cyclonic subpolar gyre. The estimated period of the loop is about 14 years (Fig. 20(b) and (c)), which is the same period of the GSA to complete its cycle. The events of both GSA and LGSA are found in the time series of CEOF mode2+3 in the LS as the two minima in around 1971 and 1983-1985, respectively (Fig. 37). According to this time series a stronger GSA appeared in 1957-1958. The model results from Häkkinen (1993) (her Fig.7(b)) showed that there were strong salinity minima, which were highly surface trapped within the upper 100 m, in 1959, 1964-1965 and 1971. The appearance of the salinity minima in 1959 in the model results roughly coincides with that deduced from the CEOF. This may be an previously unrecognized salinity event. The timing of the other salinity minima of the model also corresponds with that from CEOF.

24

Lazier (1980) and McCartney and Talley (1982) showed the Labrador Sea water steadily warmed by 0.4° C from the early 1950s through 1971 in the upper 2000 m depth. The amplitude of the warming in the time series of CEOF model (Fig. 21) is about 0.5° C, comparable to the observation. Lozier et al. (1995) and Dickson et al. (1996) documented a cooling by 0.8° C in the Labrador Sea from winter 1971 until 1990. The time series from CEOF model (Fig. 21) shows a cooling from 1966 to 1990. However, the amplitude of the cooling, about 0.3° C, is less than half of that from observation.

These changes in the ocean state might be related to changes in the overlying windstress. Variations of the windstress curl modulate the ocean gyres. The atmospheric forcing, which has basically a white spectrum, might drive a red spectrum response in the ocean's SSTA, creating decadal changes in the ocean (Frankignoul et al. (1997)). Thus the ocean exhibits inherent decadal oscillations in the form of an unstable coupled atmosphere-ocean interaction. Analysis of the windstress curl is consistent with this picture.

Pseudo windstress curl data from 1950 to 1992, from 20° N to 70° N and from 70° W to 20° E, were examined using real EOF analysis. The low-pass filter is not applied before the submission to the EOF. The curl is formed in spherical coordinates. (Pseudo wind stress is defined as $\tau = \mathbf{u}\,|\mathbf{u}|$, where $\mathbf{u} = (u, v)$ and u and v are zonal and meridional wind components, respectively.) The pseudo windstress data set was processed the same way as the windstress described above.

The first four modes account for more than 40% of the total variance, of which first mode accounts for 19% of the total variance. These are considered

25

physically significant (Fig. 5(c)). The first and the second modes (Fig. 38(a) and Fig. 39(a)) have roughly zonal structure, whereas the third and the four modes have alternating positive and negative patches (Fig. 40(a) and Fig. 41(a)). The spatial pattern of the first mode is characterized by the zonally elongated basin-wide standing oscillation with three extrema (Fig. 38(a)). The time function of the first mode exhibits the NAO signal with a correlation coefficient to the NAO index of $r=0.67$ (Fig. 38(b)). At low-frequency the spectrum of mode 1 has basically a white frequency spectrum (Fig. 38(c)). Frankignoul et al. (1997) showed similar results in an analysis of the first four EOFs of windstress curl fields calculated from model results of ECHAM1/LSG in the North Atlantic. Although the wind stress curl is considered stochastic with a white frequency spectrum, the SSTA exhibits inherent oscillations with a red spectrum at decadal time scales. A correlation between wind forcing and SSTA was found only in the Labrador Sea region in this analysis.

The present study examines decadal changes in North Atlantic SSTA. The temporal evolution of the multi-decadal patterns were not fully understood because the high-coverage data are too short to give the required information, whereas, the quasi-decadal timeseries are long enough to analyze over several cycles. Further numerical model and theoretical studies would compensate for the shortcomings of the data.

26
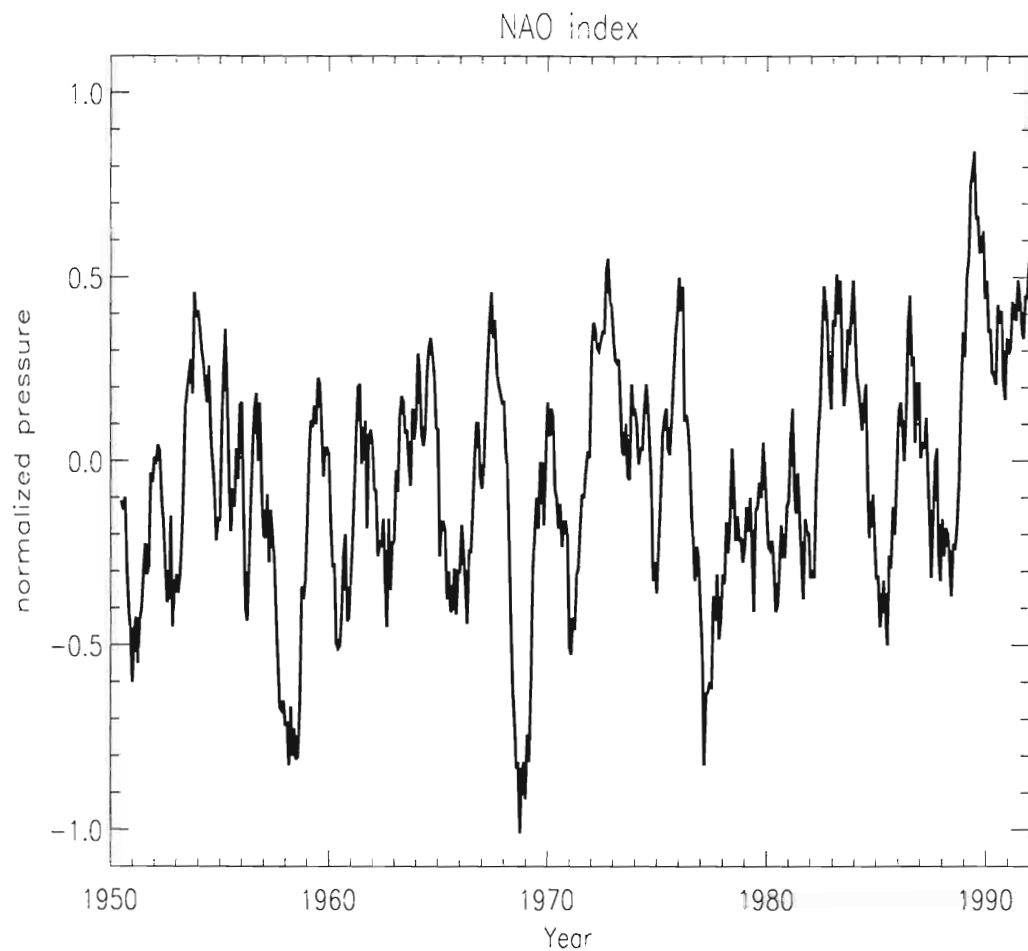
6. FIGURES

Figure 1:   Normalized time series of North Atlantic Oscillation (NAO) from 1950 to 1992 (from the Climate Prediction Center). It is the difference of normalized pressures between Lisbon, Portugal and Stykkisholmur, Iceland. This is the result of a low-pass filter (>12 months).

28

Climatology of Ekman plus Model Currents
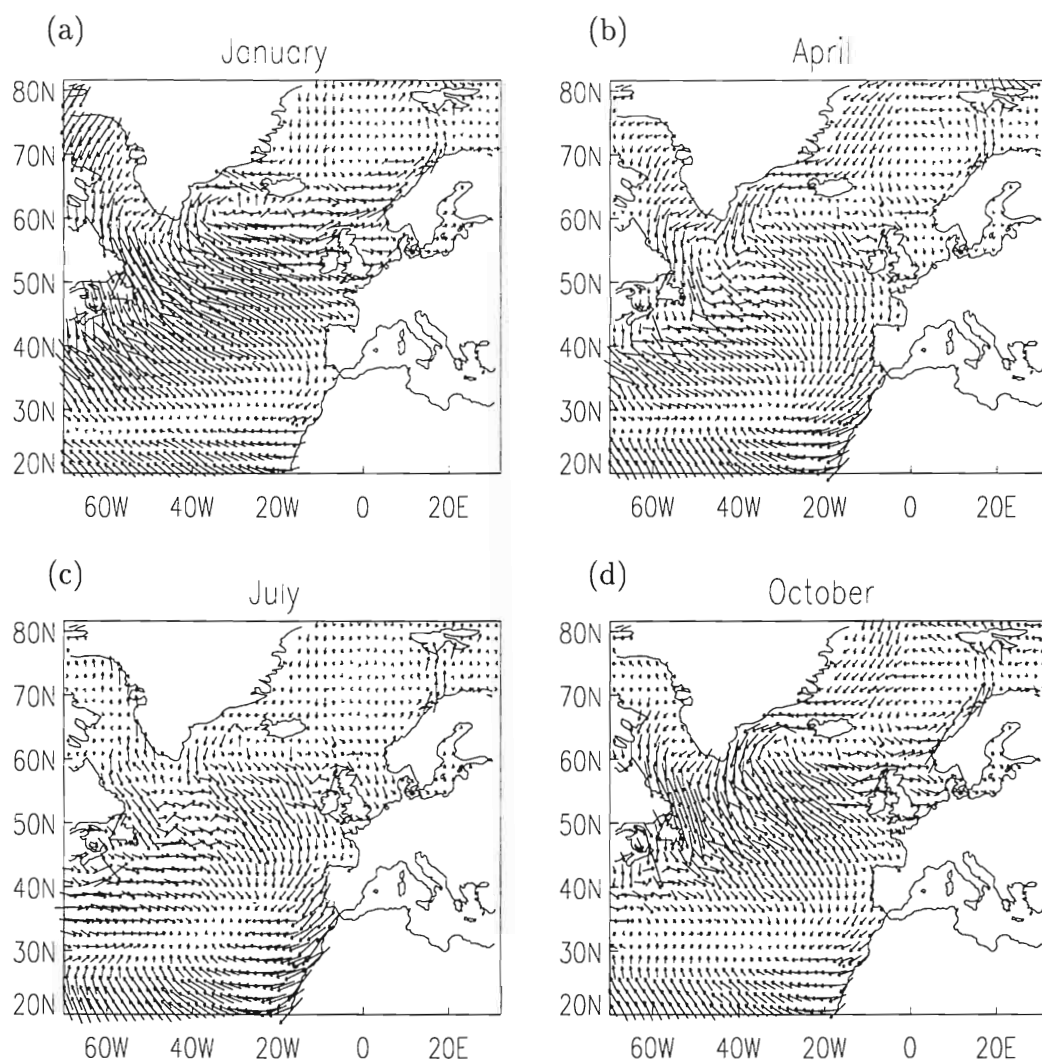
Figure 2: Climatology of model and Ekman currents. The model currents are provided by S. Häkkinen and Ekman currents are calculated from the climatology of windstress. (a) January, (b) April, (c) July, (d) October

29

Sea Surface Temperature in 1949

(a) January

(b) April
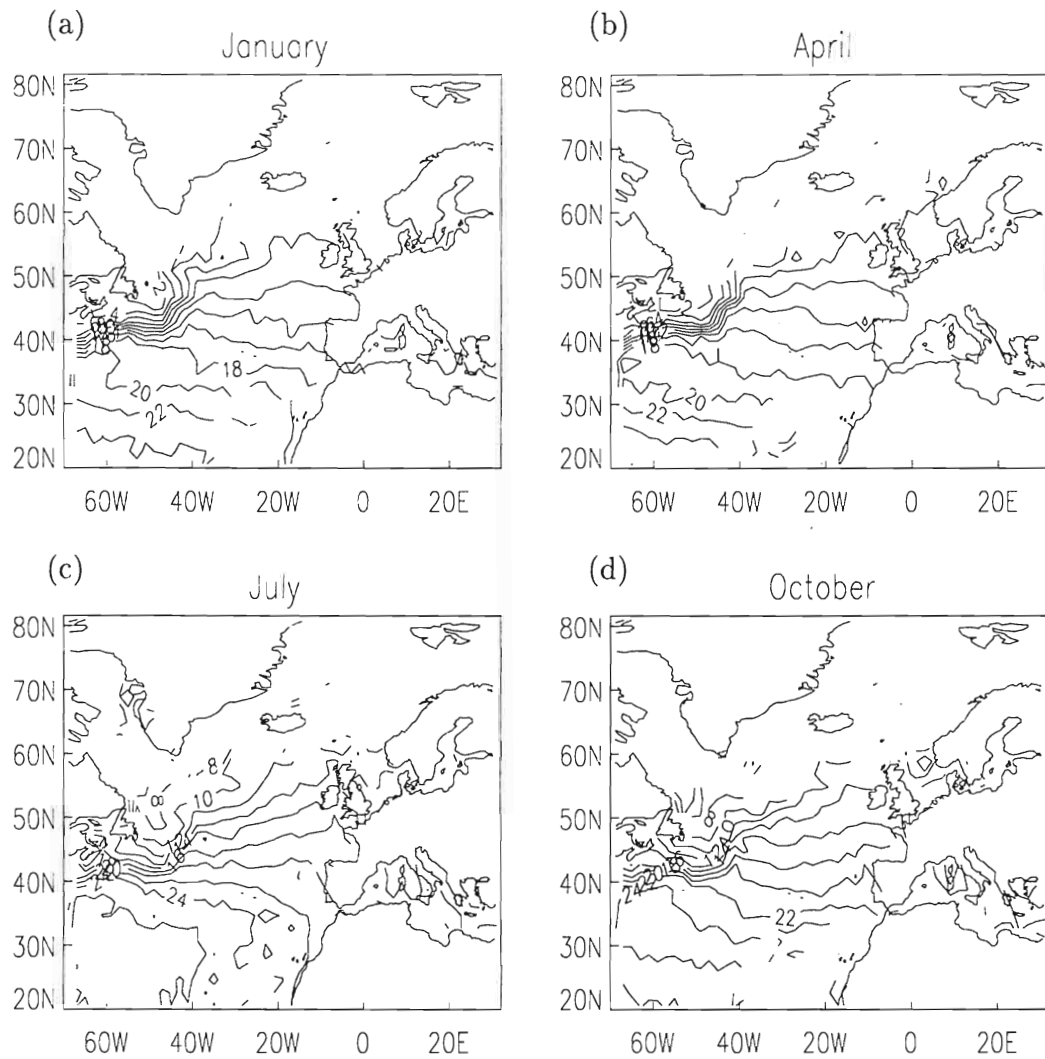
(c) July

(d) October

Figure 3:   Sea surface temperature of raw data in 1949. Isobath intervals are 2° C. (a) January, (b) April, (c) July, (d) October

30

Sea Surface Temperature Climatology
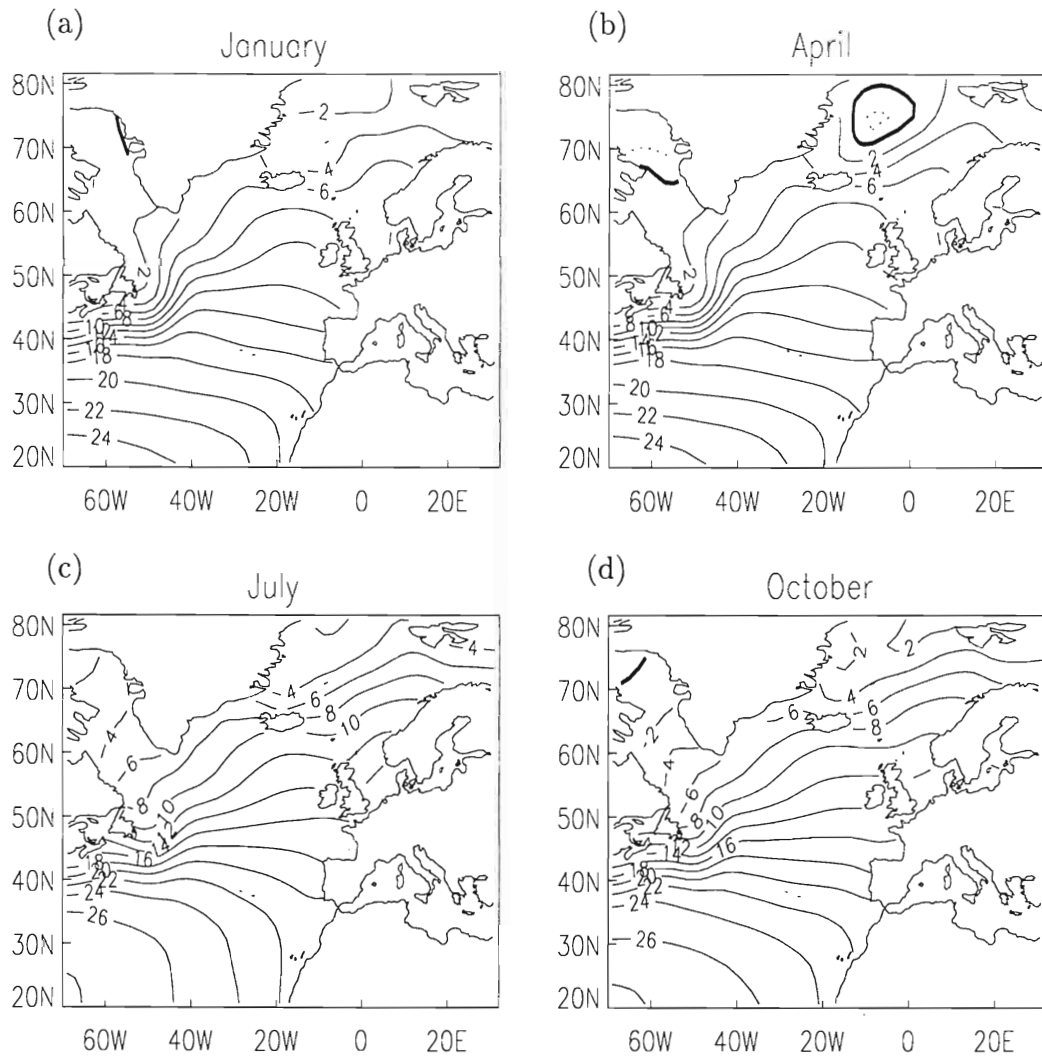
Figure 4: Monthly averaged sea surface temperature climatology. Isobath intervals are 2° C for the positive values and 1° C for the negative values. (a) January, (b) April, (c) July, (d) October

31
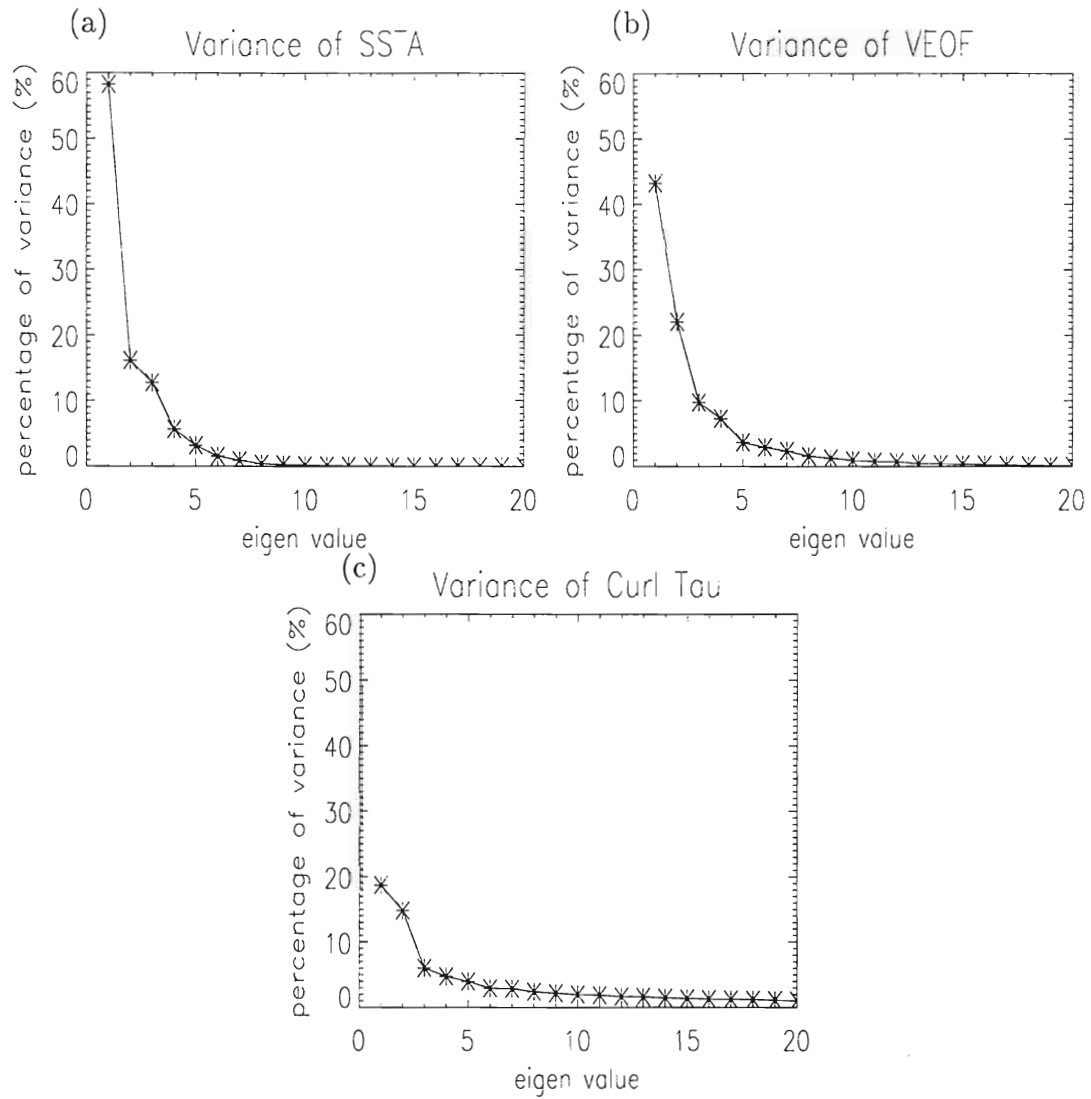
Figure 5: Eigenvalue spectrum (in percent of explained variance) of (a) SSTA (b) VEOF (C) curlτ, respectively.

Chronology of SSTA (CEOF Mode1)
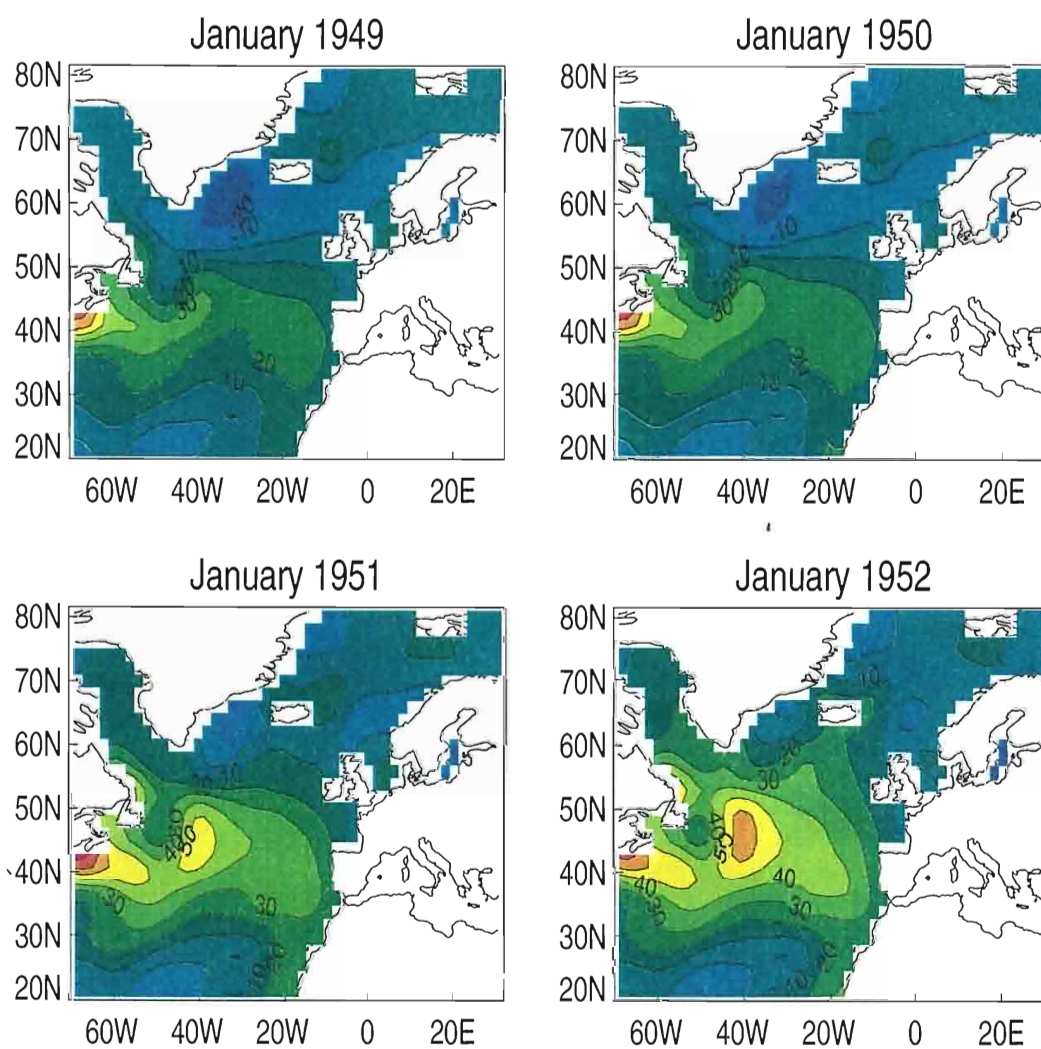
Figure 6: Chronological sequence of January SST anomalies after 4 year low-pass filtering obtained from CEOF mode1.

Chronology of SSTA (CEOF Mode1)
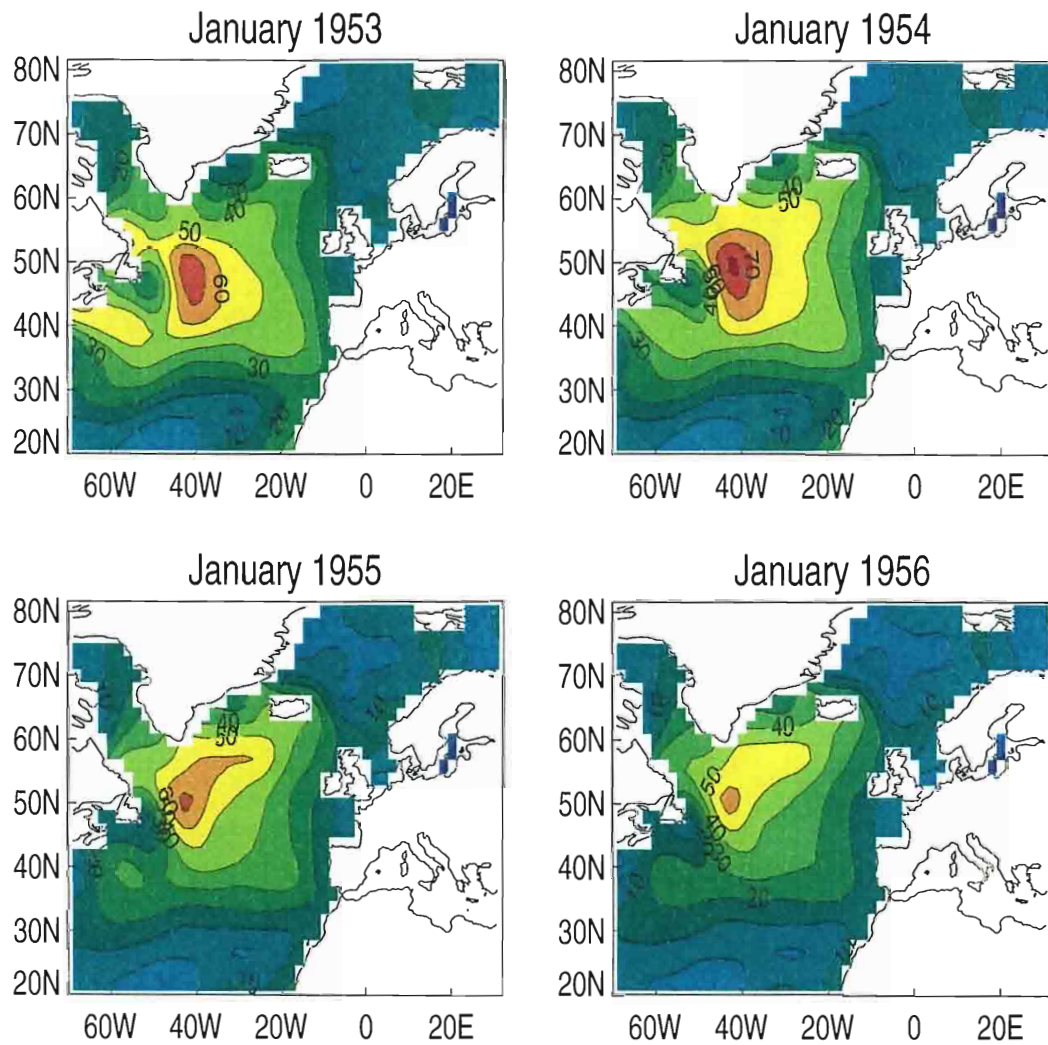
Figure 7: (continued)

Chronology of SSTA (CEOF Mode1)
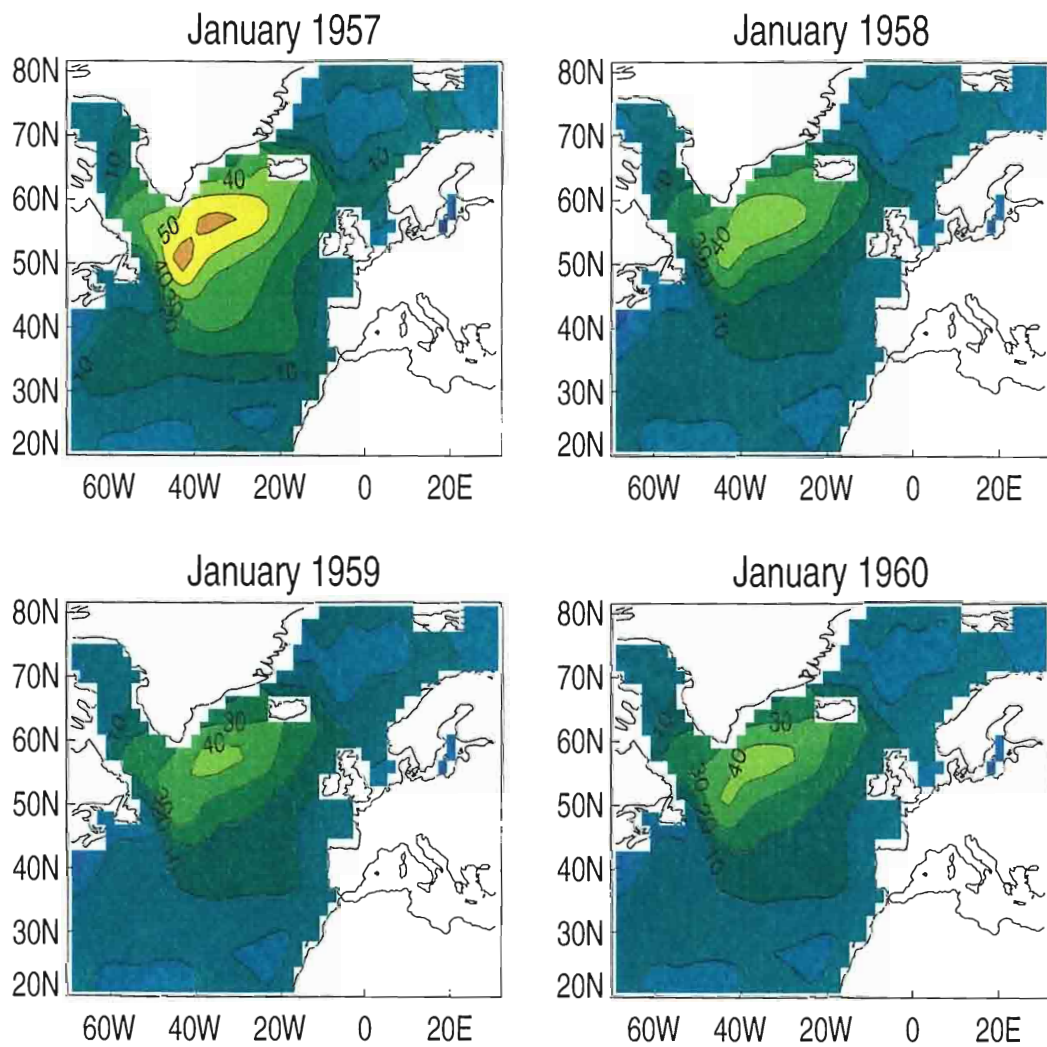
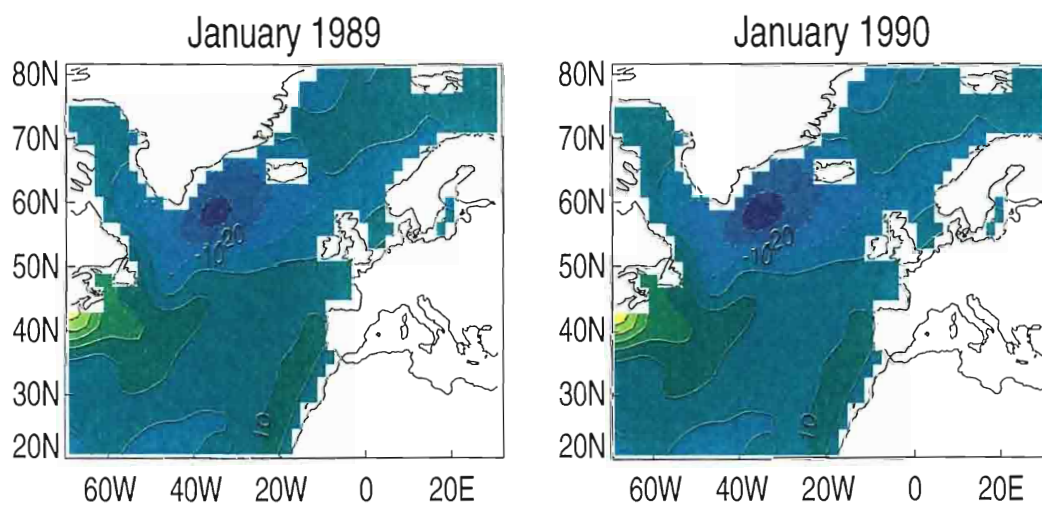
Figure 8:   (continued)

# Chronology of SSTA (CEOF Mode1)
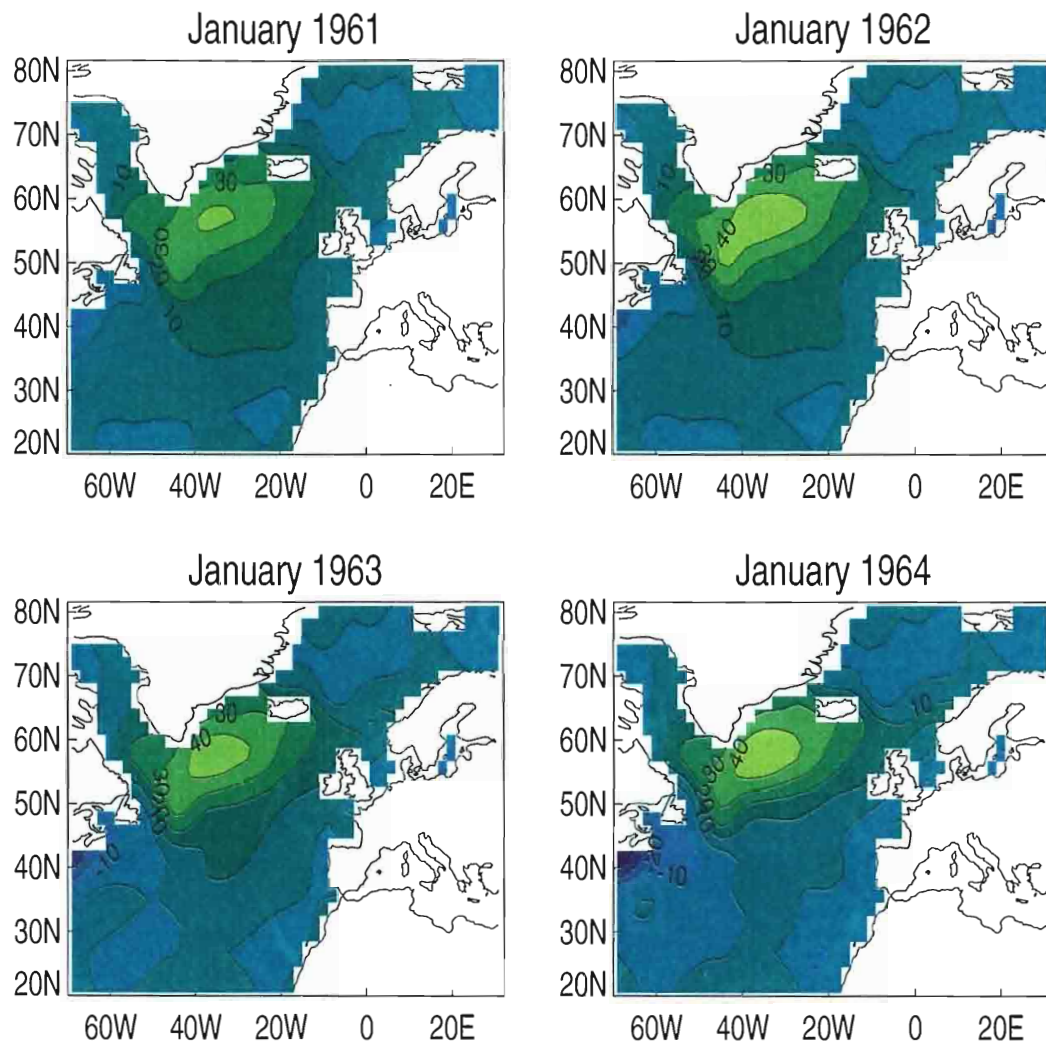
Figure 9:   (continued)

Chronology of SSTA (CEOF Mode1)
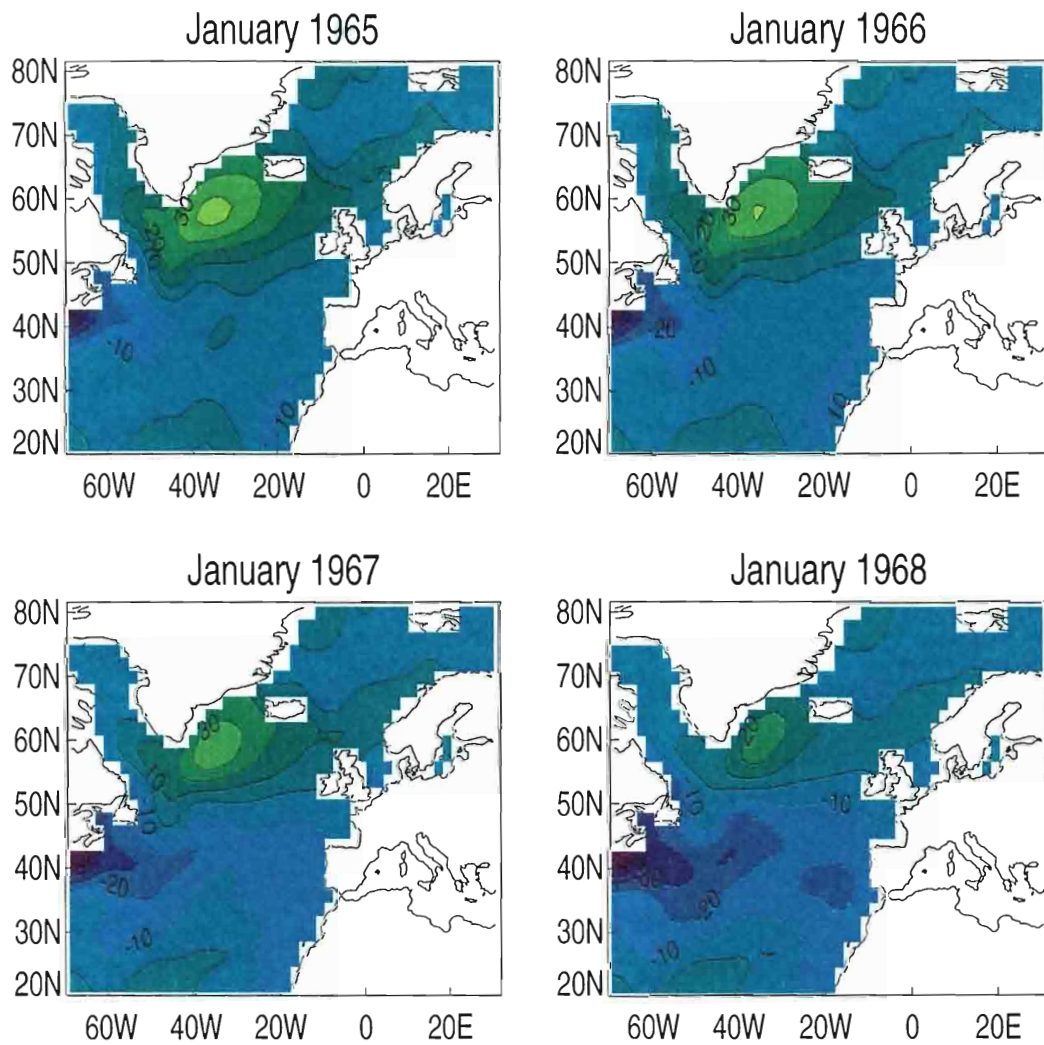
Figure 10: (continued)

Chronology of SSTA (CEOF Mode1)
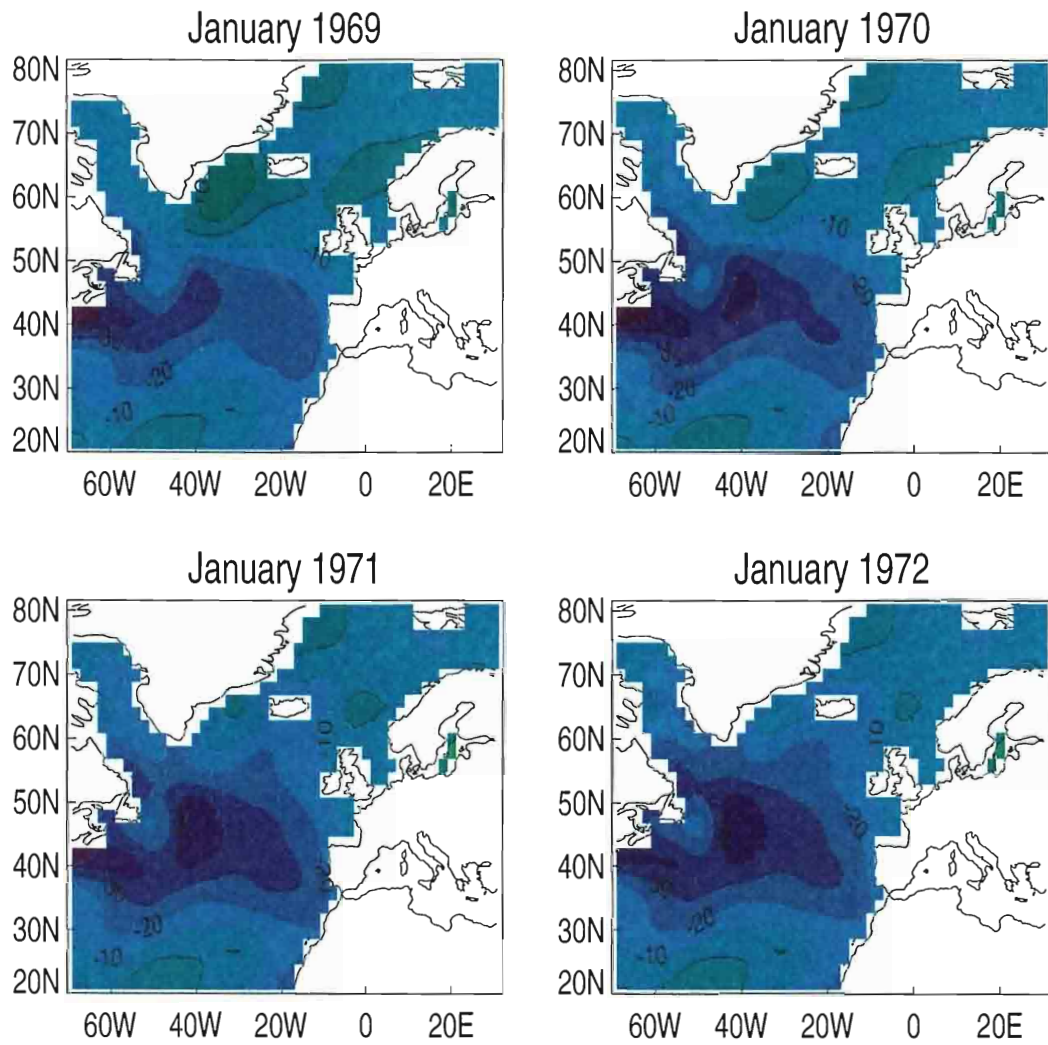
Figure 11: (continued)

Chronology of SSTA (CEOF Mode1)
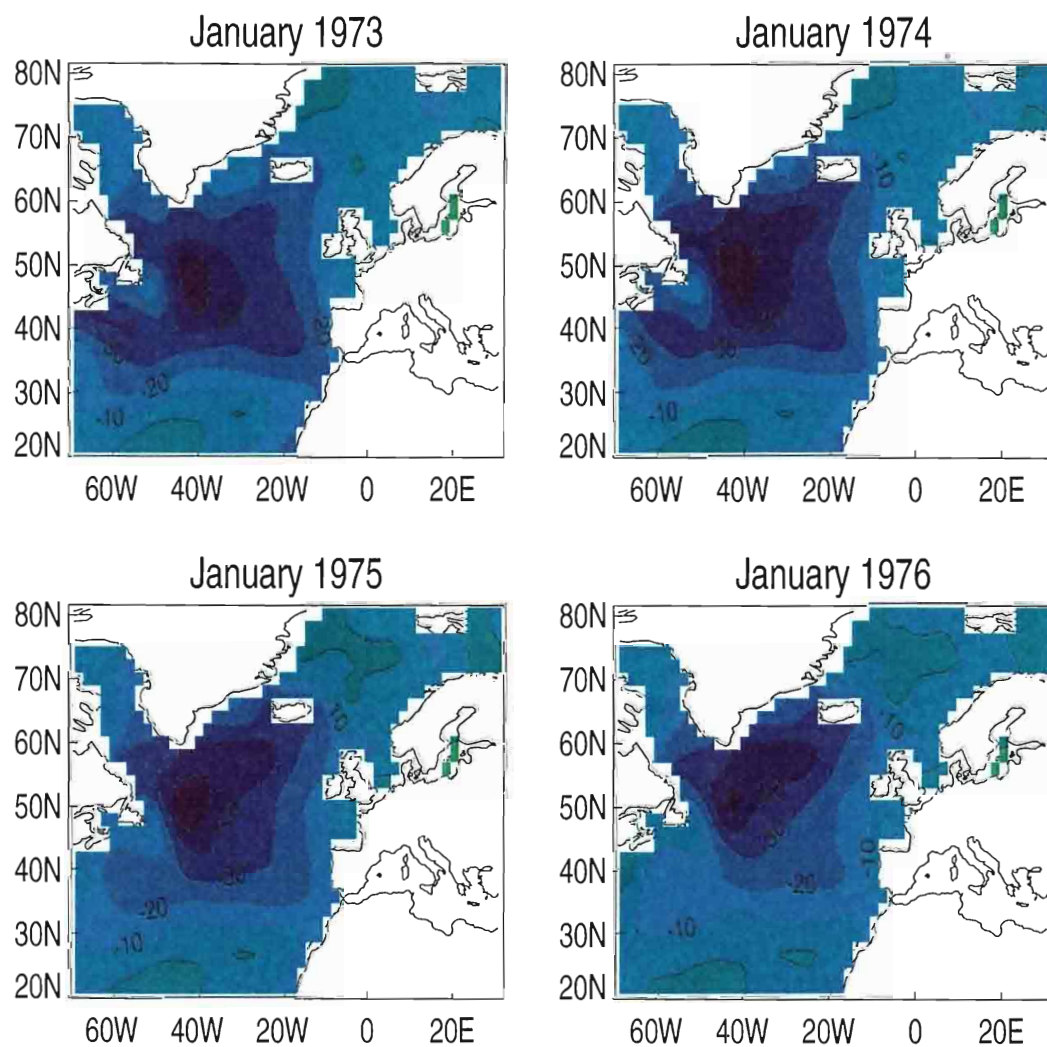
Figure 12:   (continued)

Chronology of SSTA (CEOF Mode1)

January 1977

January 1978

January 1979

January 1980
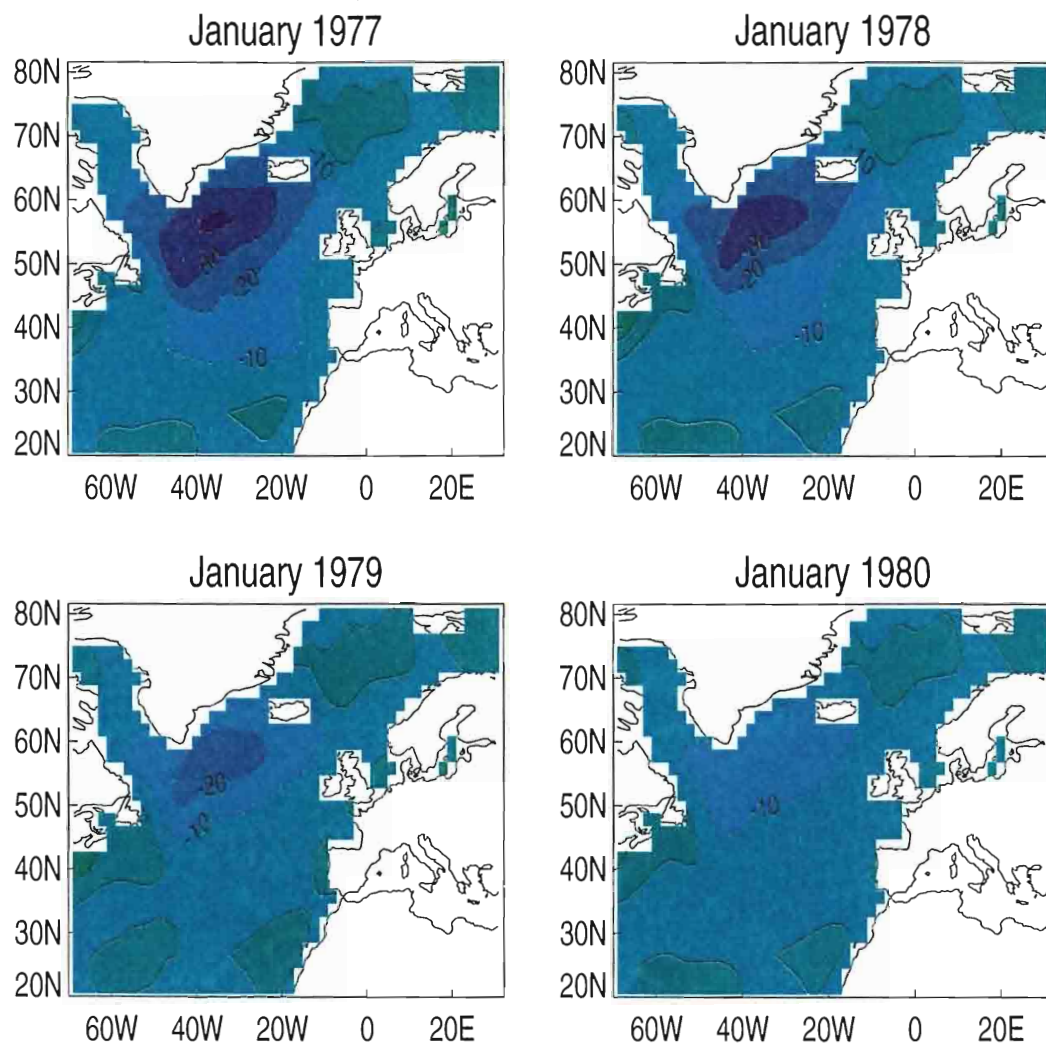
Figure 13:   (continued)

Chronology of SSTA (CEOF Mode1)

January 1981

January 1982

January 1983

January 1984
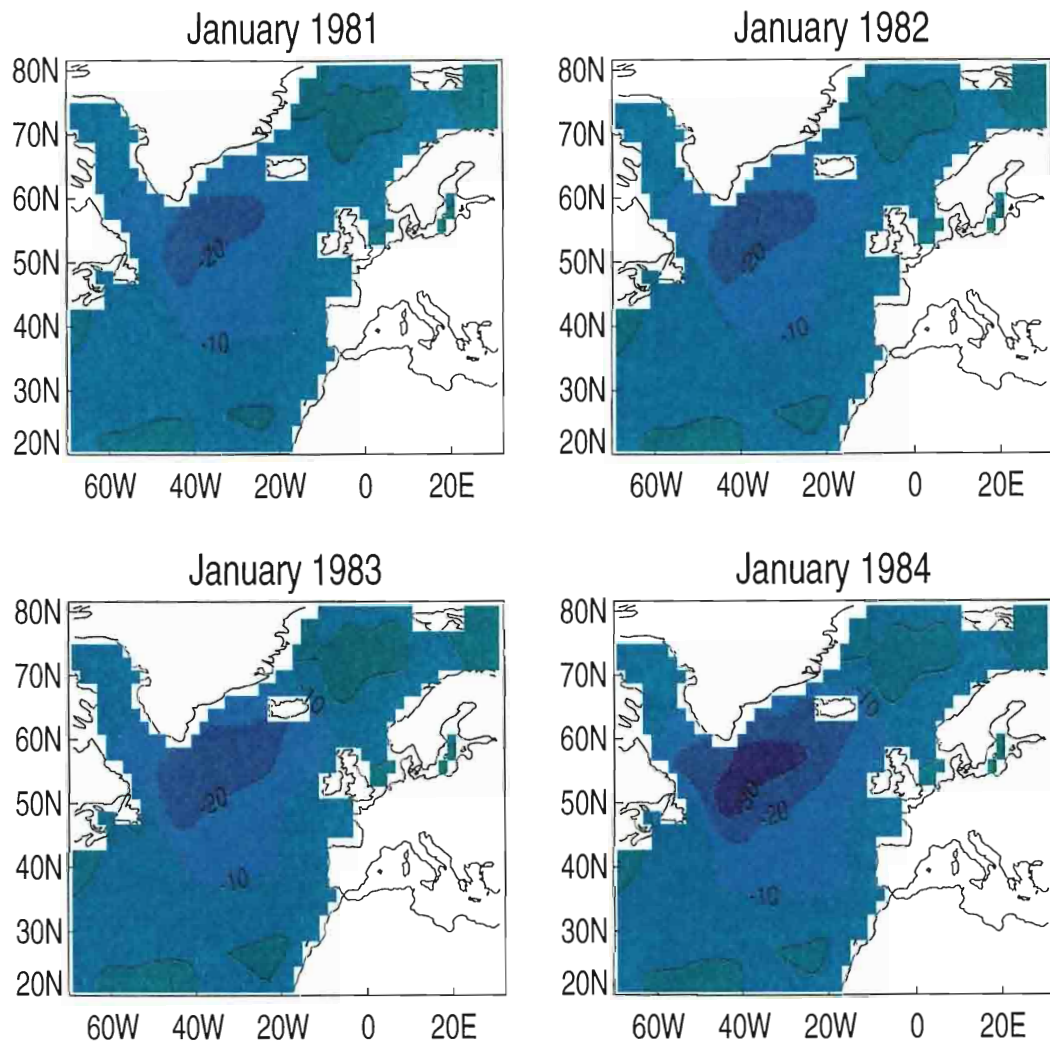
Figure 14:   (continued)

Chronology of SSTA (CEOF Mode1)
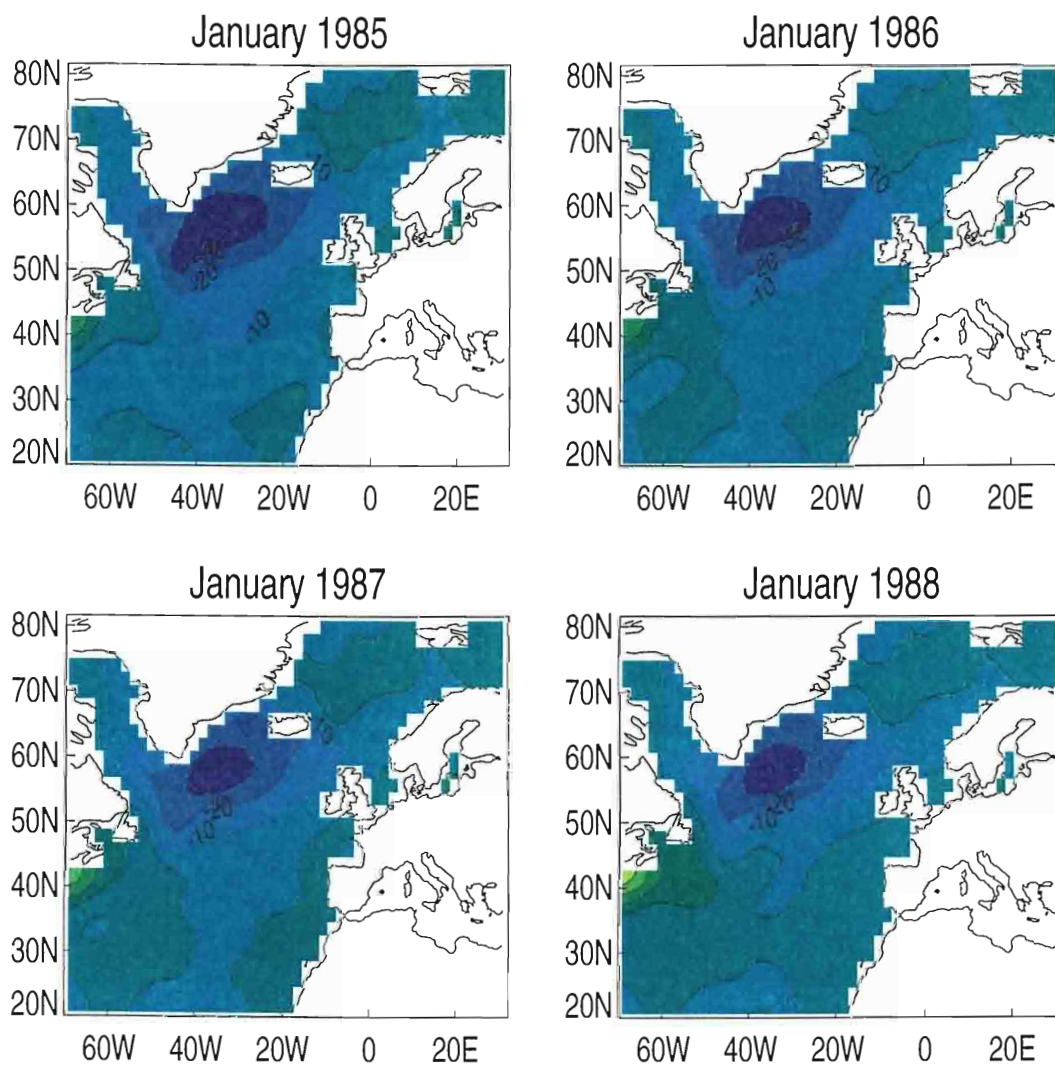
Figure 15: (continued)

Chronology of SSTA (CEOF Mode1)

Figure 16: (continued)

Spatial Amplitude Function
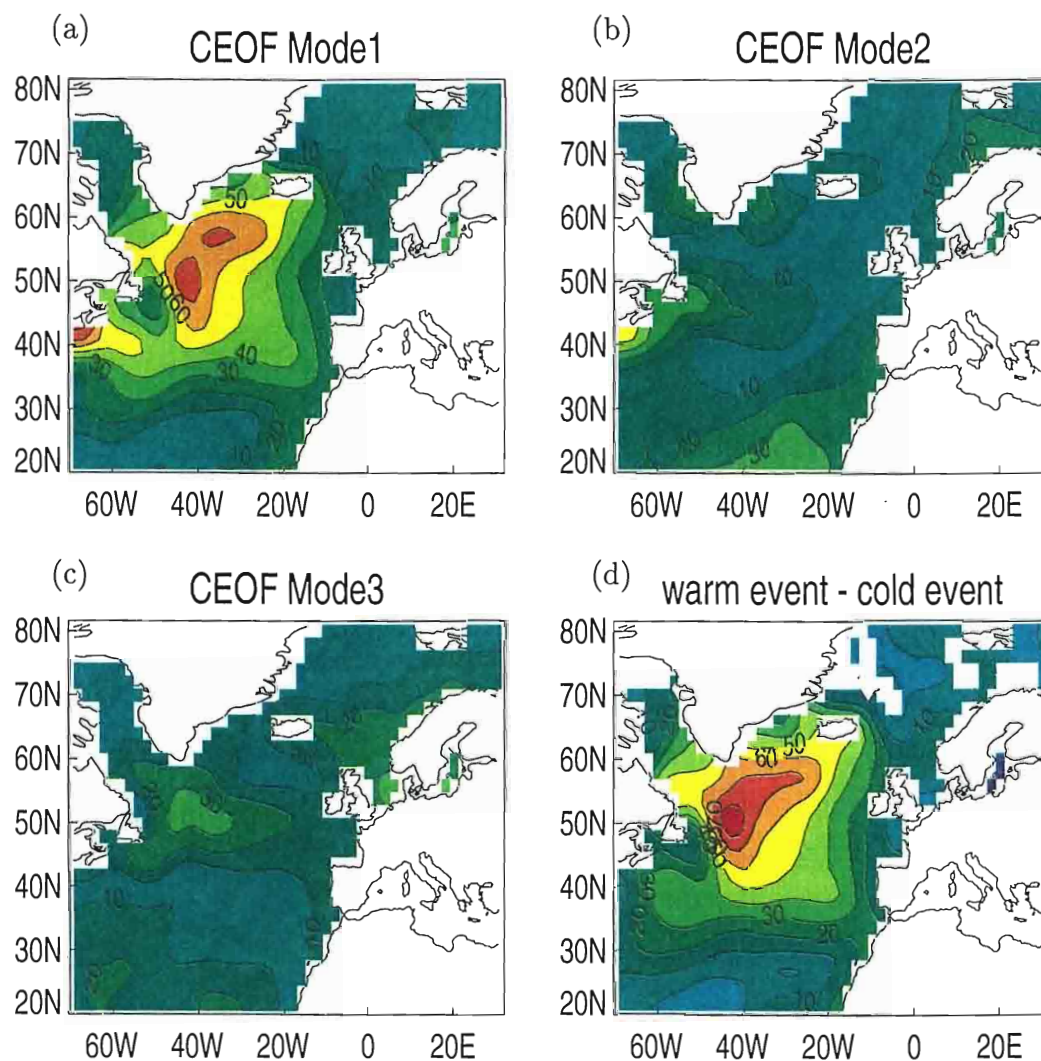
Figure 17: Spatial amplitude functions obtained from CEOF. (a), (b), (c) correspond to mode1, mode2 and mode3, respectively. (d) is a SSTA trend of averaged warm event (1950-1964) minus cold event (1970-1984).

44

Spatial Phase Function
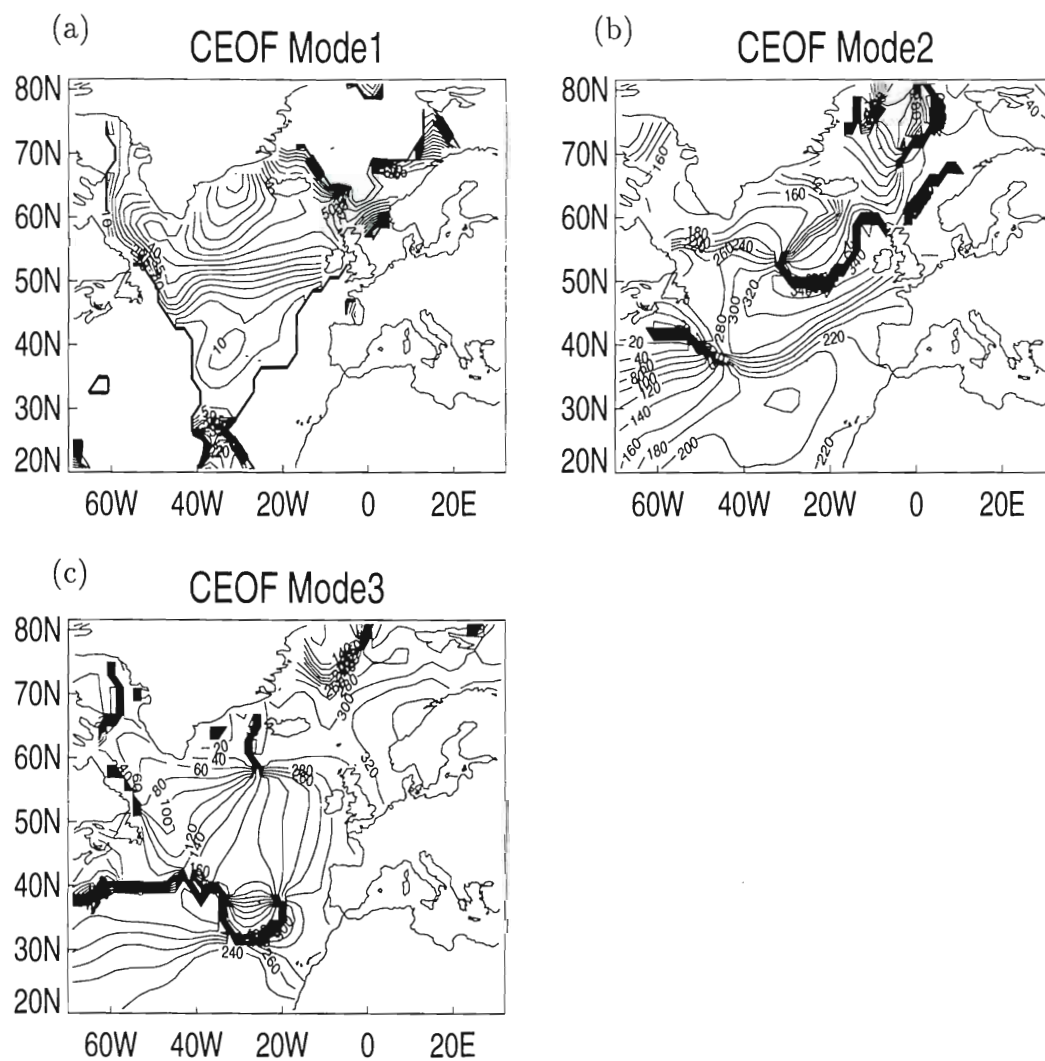
Figure 18: Spatial phase functions obtained from CEOF. (a), (b), (c) correspond to mode1, mode2 and mode3, respectively. For the mode 1 only the phase from 0° to 80° is shown in order to highlight the region of interest.
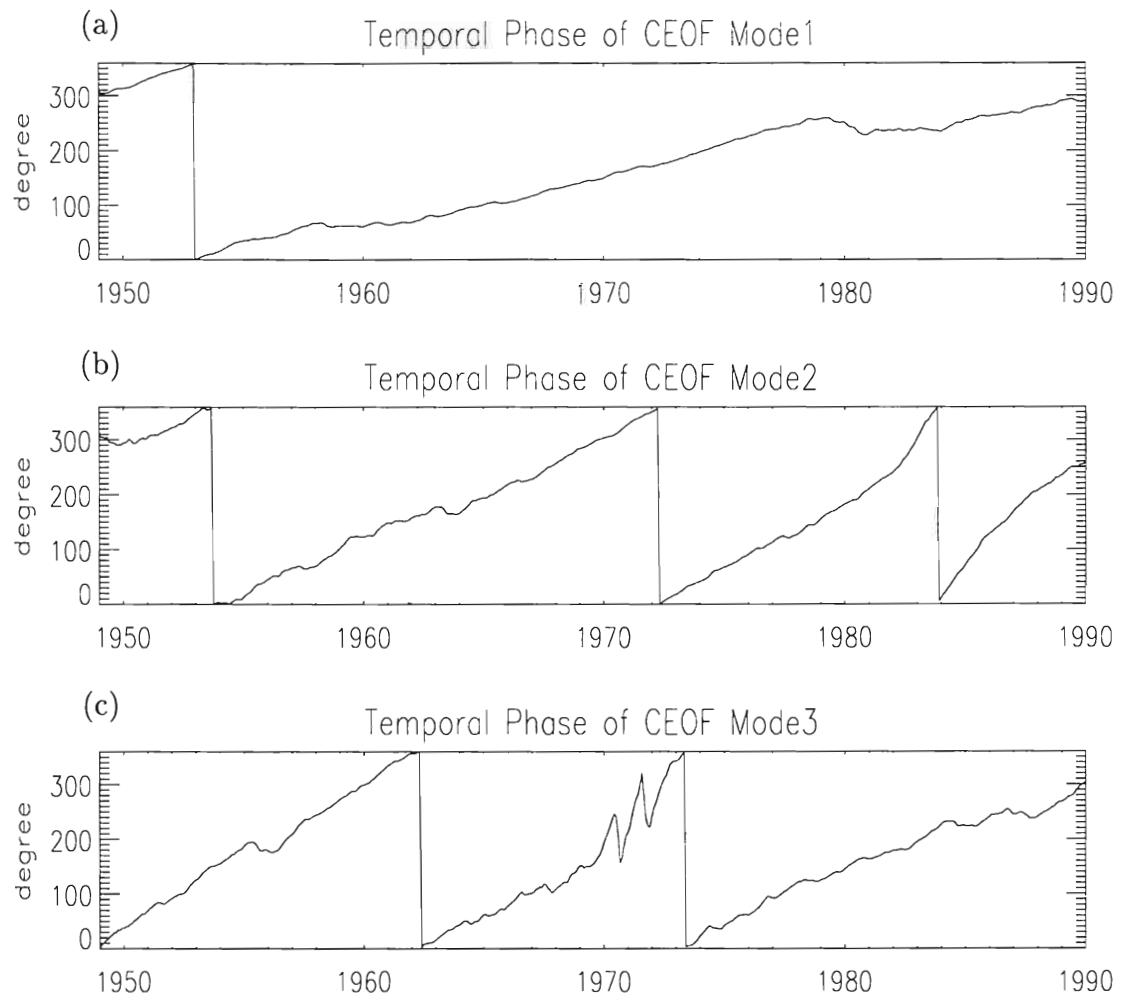
Figure 19:   Temporal phase functions obtained from CEOF. (a), (b), (c) correspond to mode1, mode2 and mode3, respectively. x axis is a time axis from 1949 to 1990 and y axis is an argument of the phase functions in degree (from $0°$ to $360°$).

46

Phase of CEOF Mode1

1400
1200
1000
800
600
400
200
0

degree

a = 332.700 (deg)
b = 0.686
y = a + bx
1 cycle = 43.7 year

(b)1950   1960Phase of CEOF Mode2 1980   1990

1400
1200
1000
800
600
400
200
0

degree

a = 193.986 (deg)
b = 2.083
y = a + bx
1 cycle = 14.4 year

(c)1950   1960Phase of CEOF Mode3 1980   1990

1400
1200
1000
800
600
400
200
0

degree

a = 19.413 (deg)
b = 2.162
y = a + bx
1 cycle = 13.9 year

1950   1960   1970   1980   1990
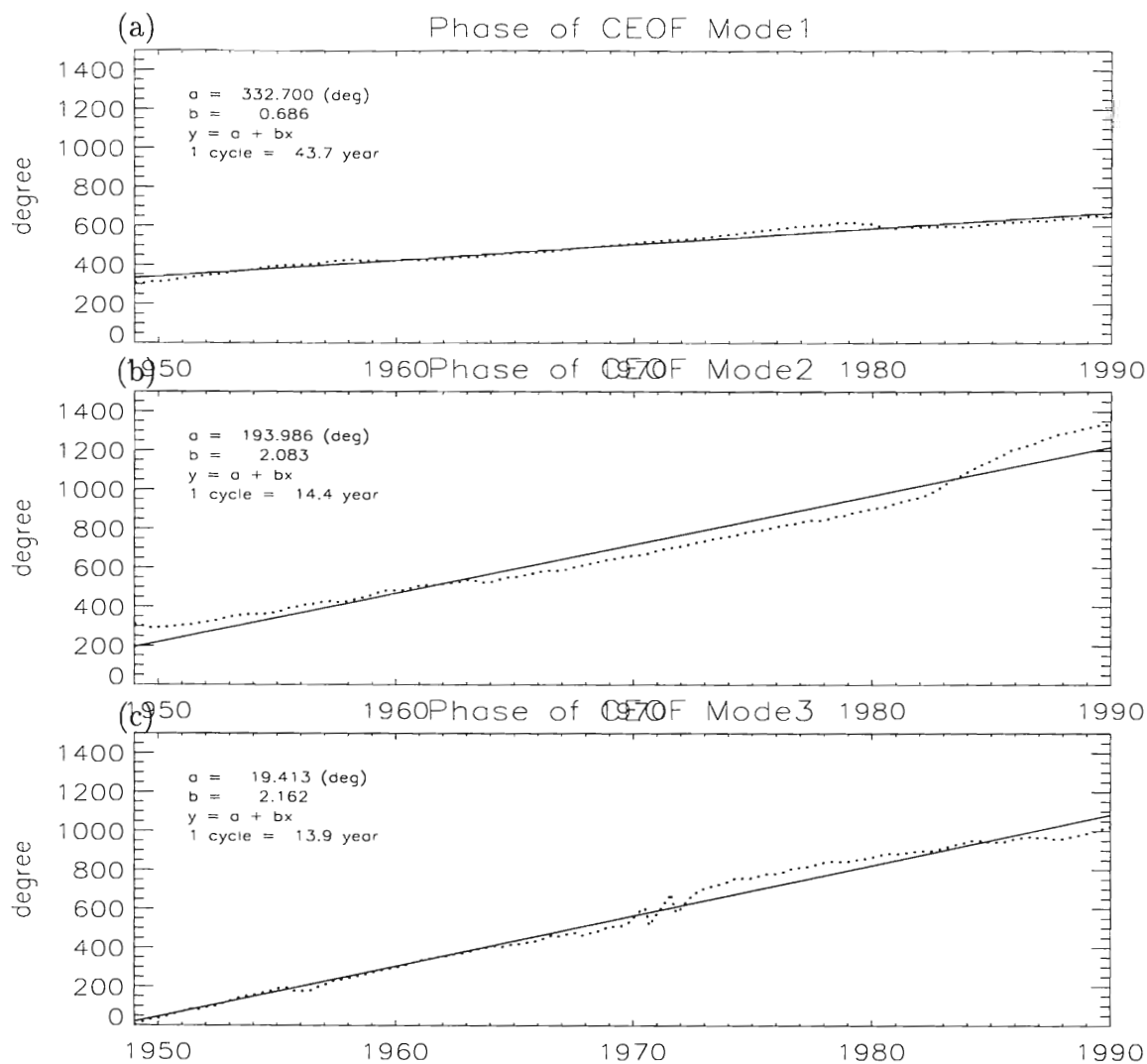
Figure 20:   Temporal phase functions obtained from CEOF. (a), (b), (c) correspond to mode1, mode2 and mode3, respectively. Dotted lines are phase functions obtained from CEOF. Solid lines are best linear-fit to the fuctions. a is a y intersept and b is the slope of the best fit function. $y = a + bx$ represents the linear function. Reciprocal of the slope is a period to complete one cycle.
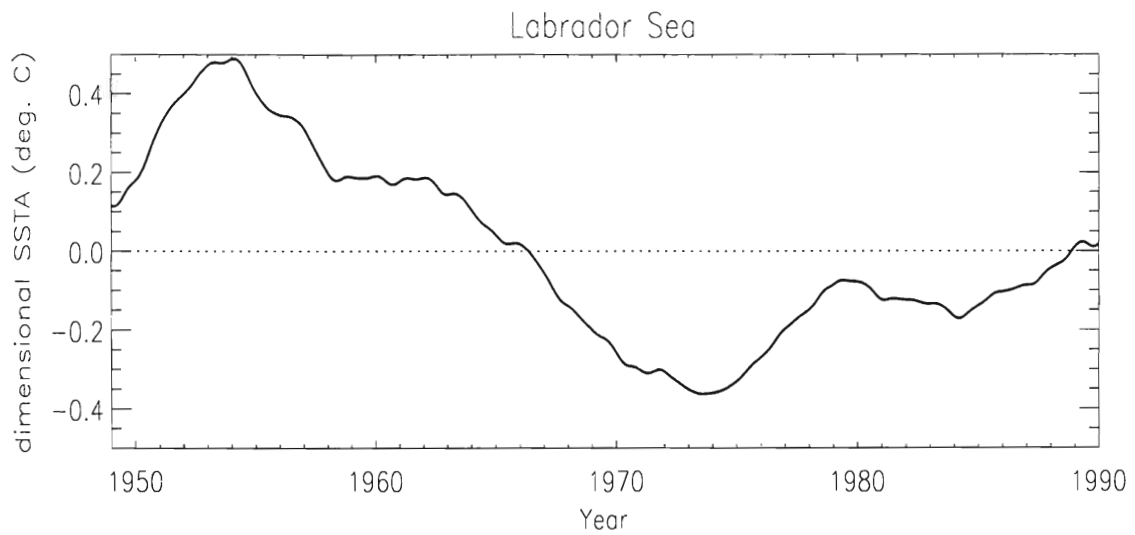
Figure 21: Sea surface temperature anomaly time series in Labrador Sea region. Time series obtained from CEOF model averaged over the Labrador region (50° N - 60° N and 60° W - 50° W). The time series is not normalized.
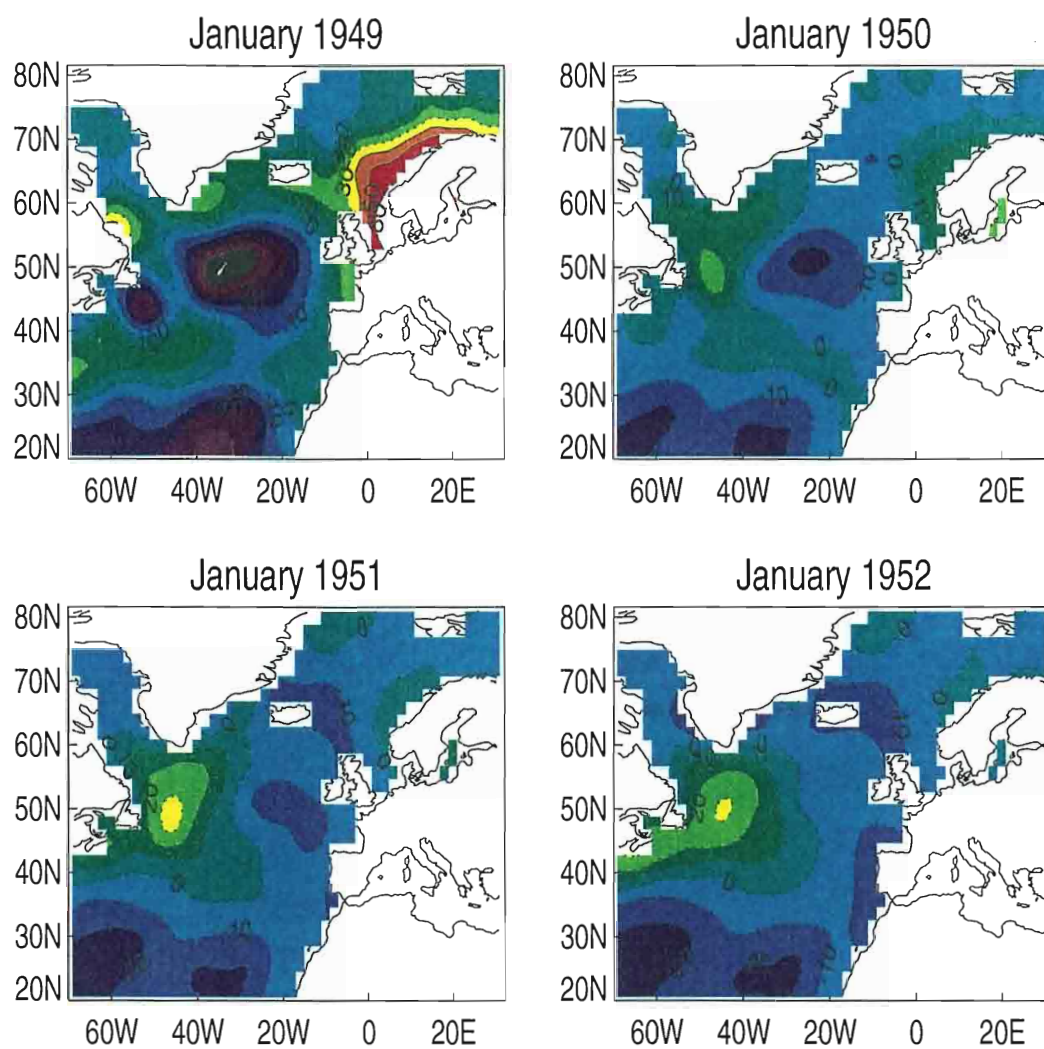
48

Chronology of SSTA (CEOF Mode2+3)

Figure 22: Chronological sequence of January SST anomalies after 4 year low-pass filtering obtained from CEOF mode1.
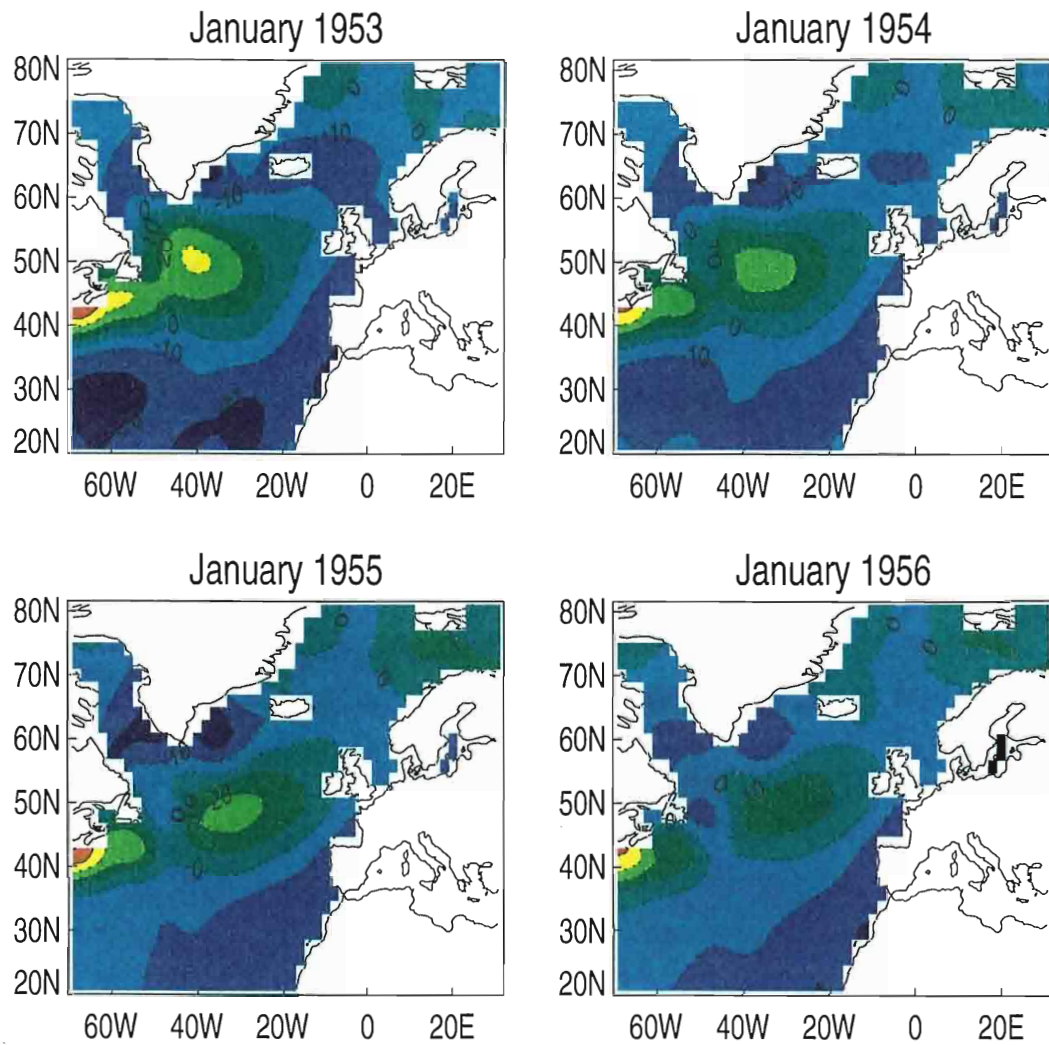
Chronology of SSTA (CEOF Mode2+3)
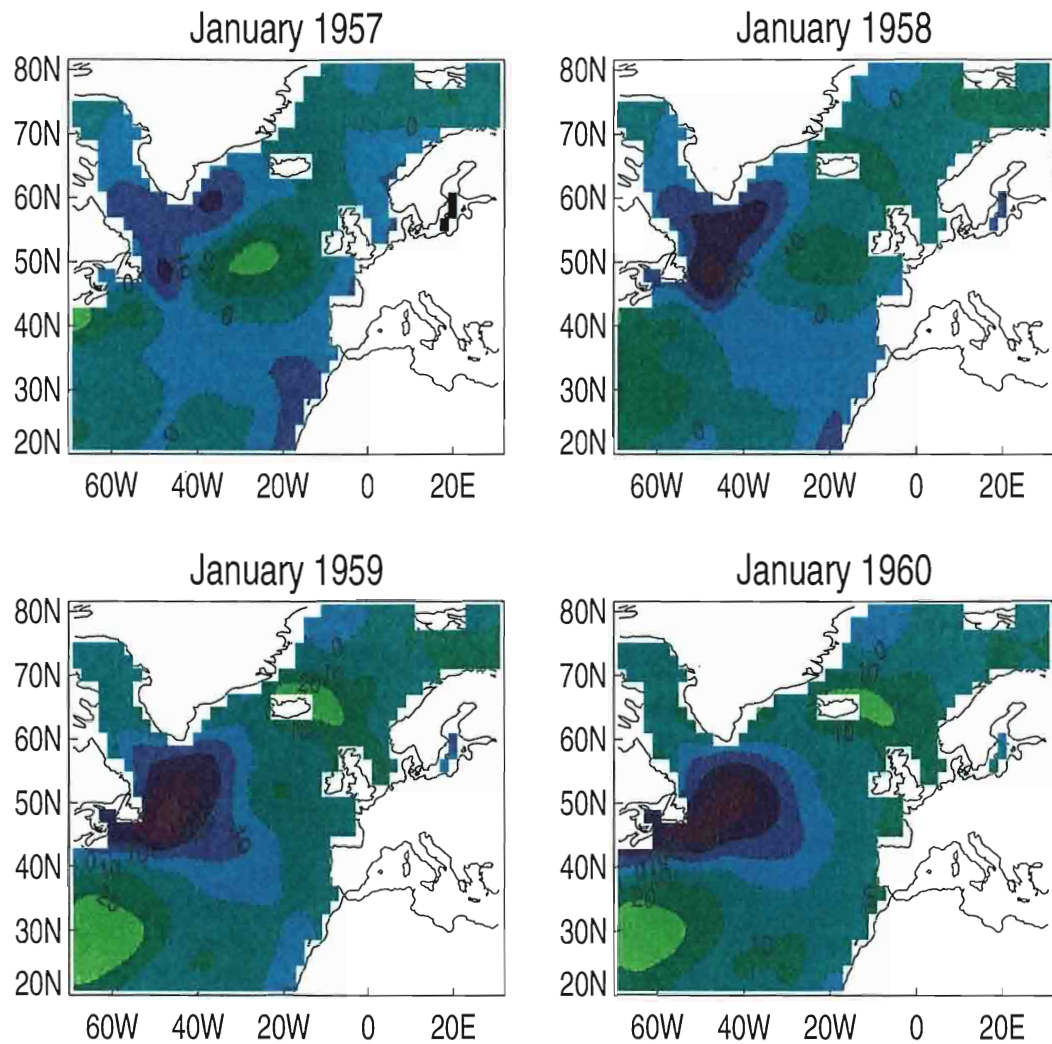

Figure 23: (continued)

Chronology of SSTA (CEOF Mode2+3)

Figure 24:   (continued)

Chronology of SSTA (CEOF Mode2+3)
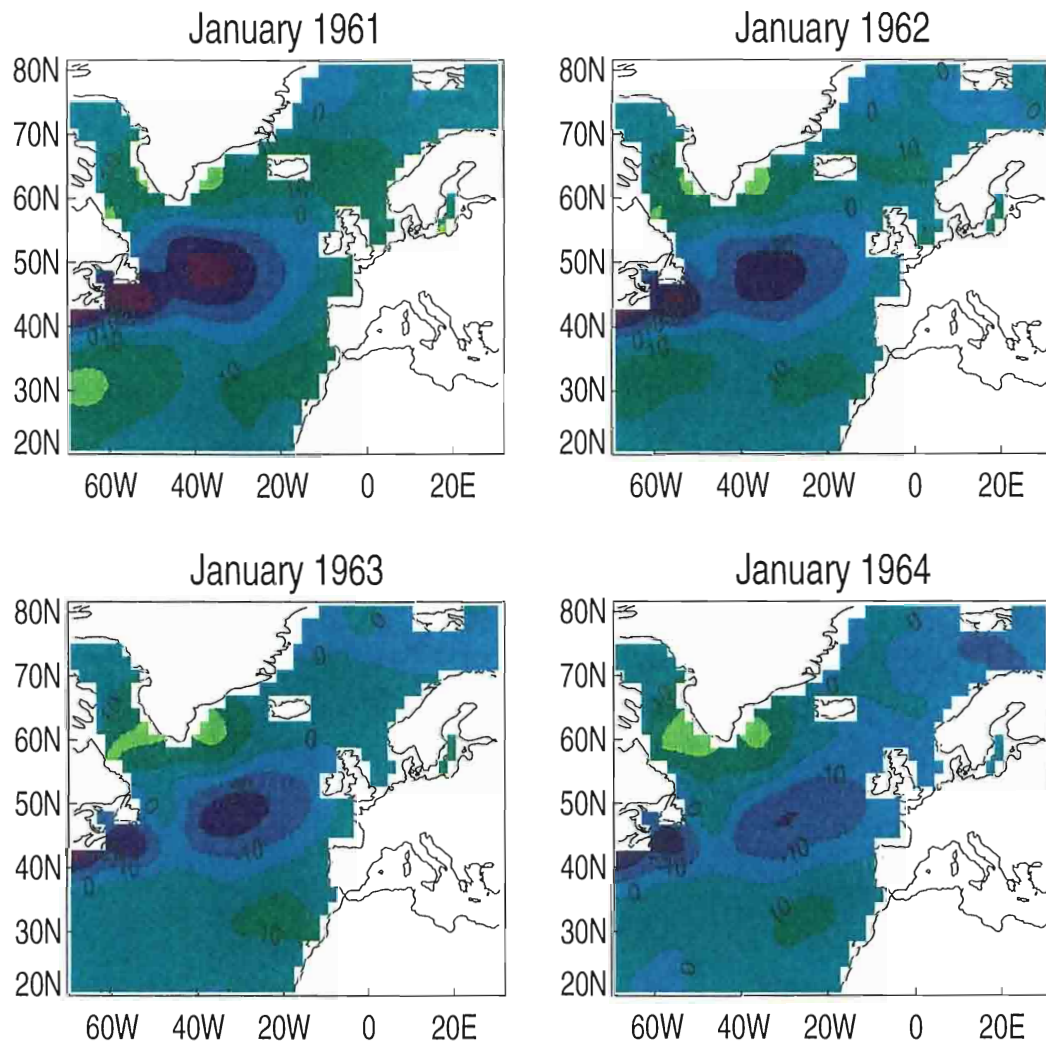
Figure 25: (continued)

Chronology of SSTA (CEOF Mode2+3)
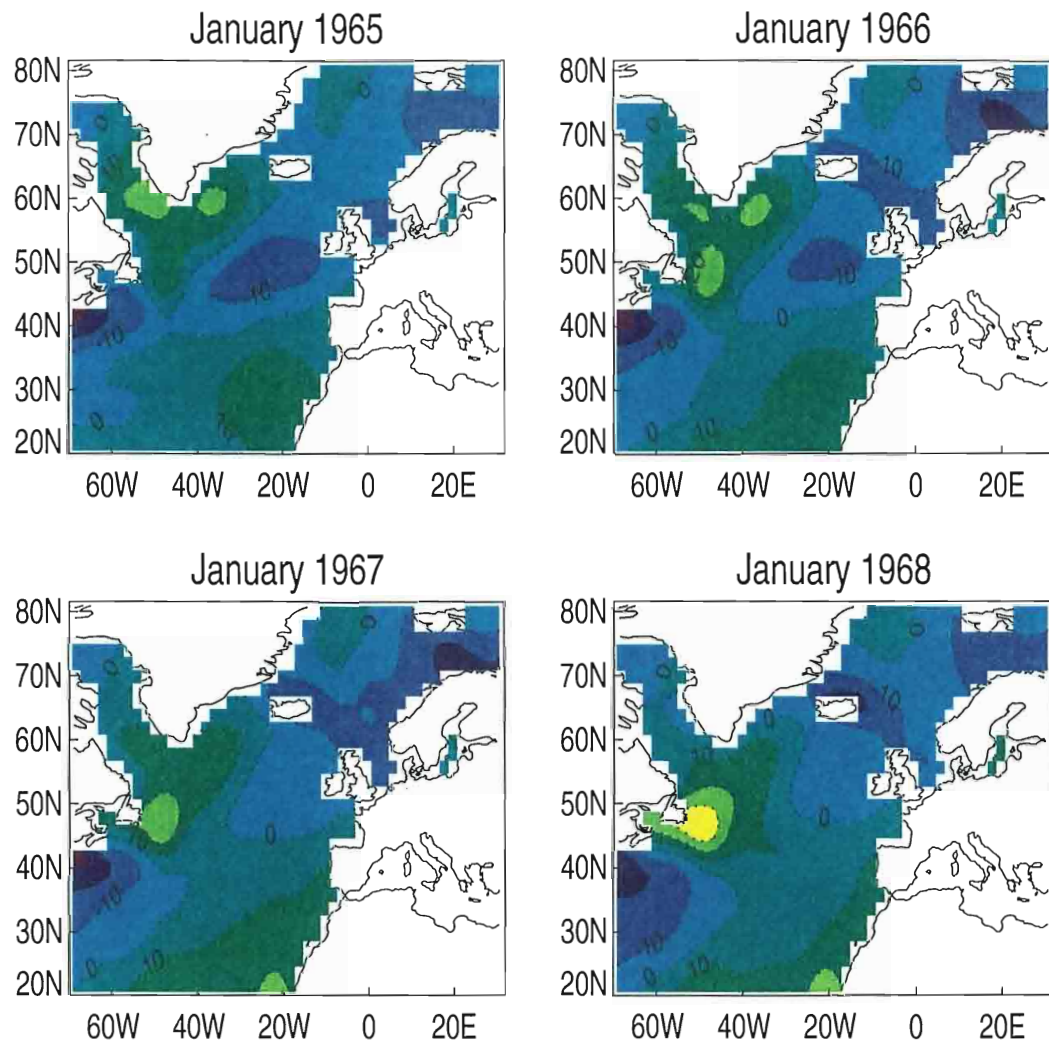
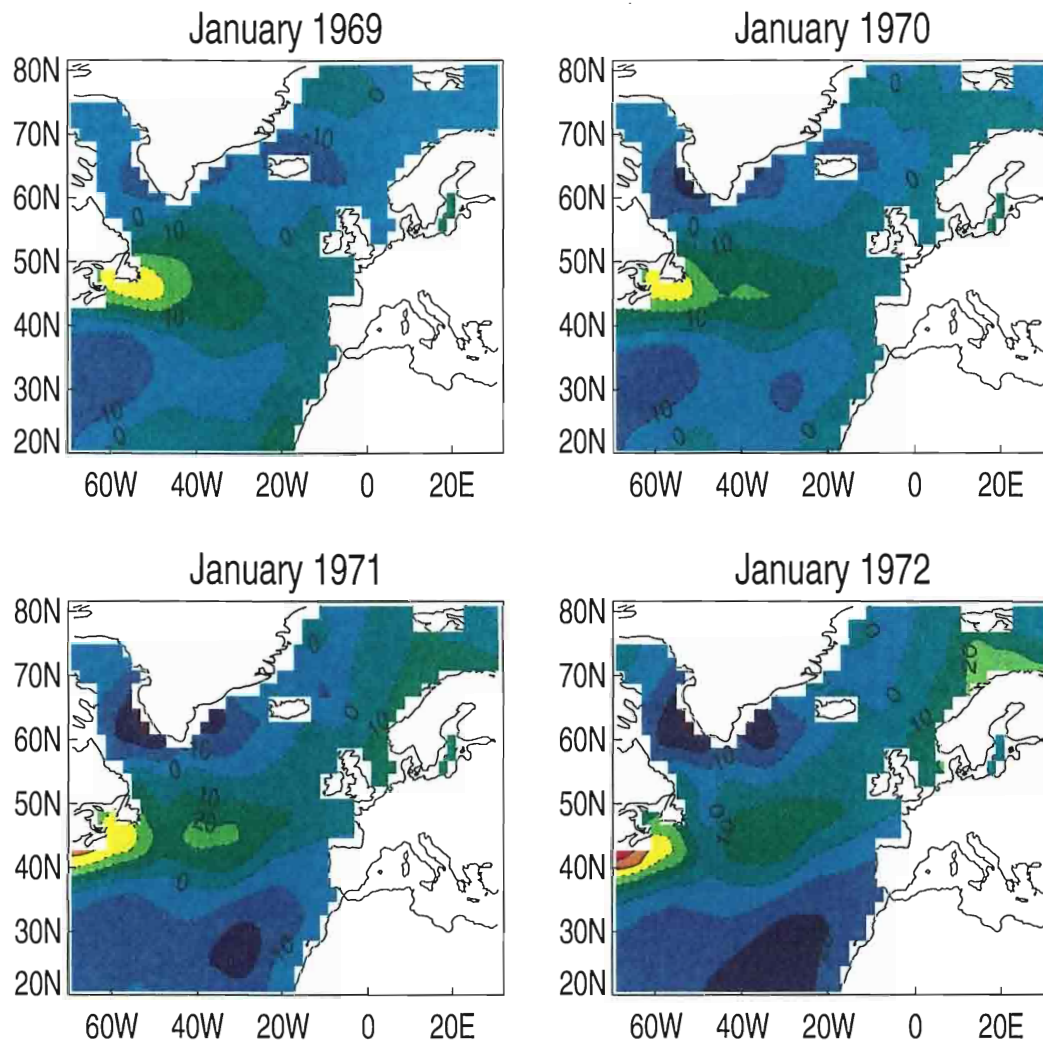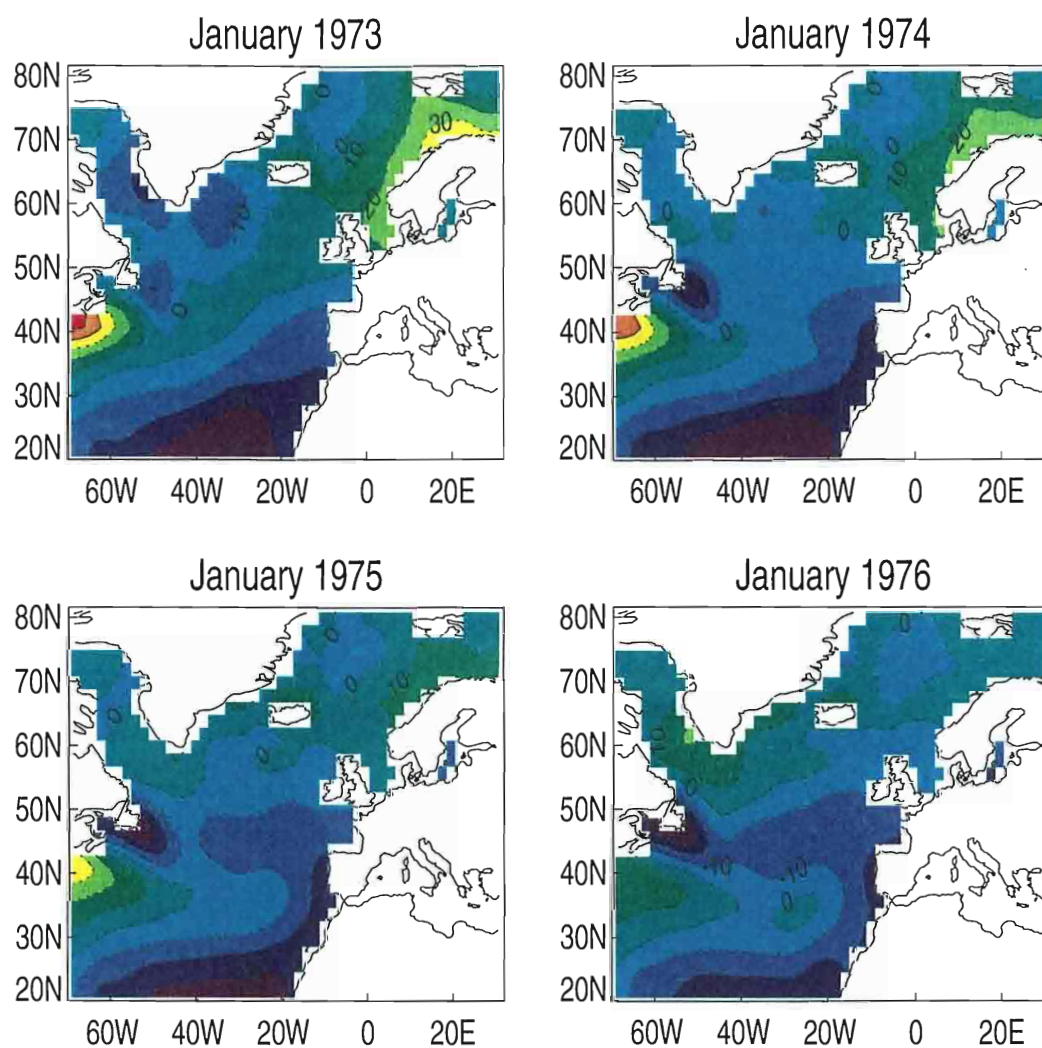Figure 26: (continued)

Chronology of SSTA (CEOF Mode2+3)

Figure 27: (continued)

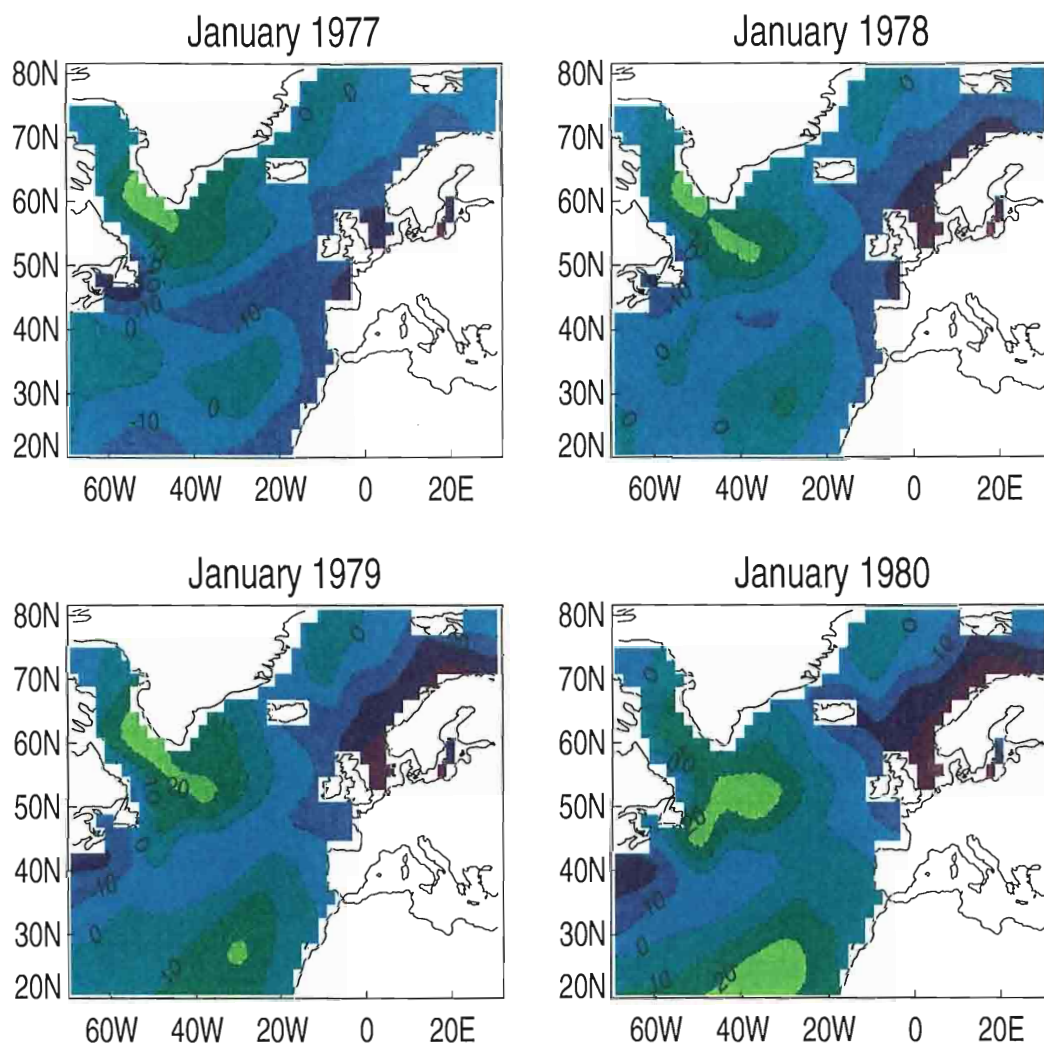# Chronology of SSTA (CEOF Mode2+3)

January 1973

January 1974

January 1975

January 1976

Figure 28: (continued)

Chronology of SSTA (CEOF Mode2+3)

Figure 29:   (continued)

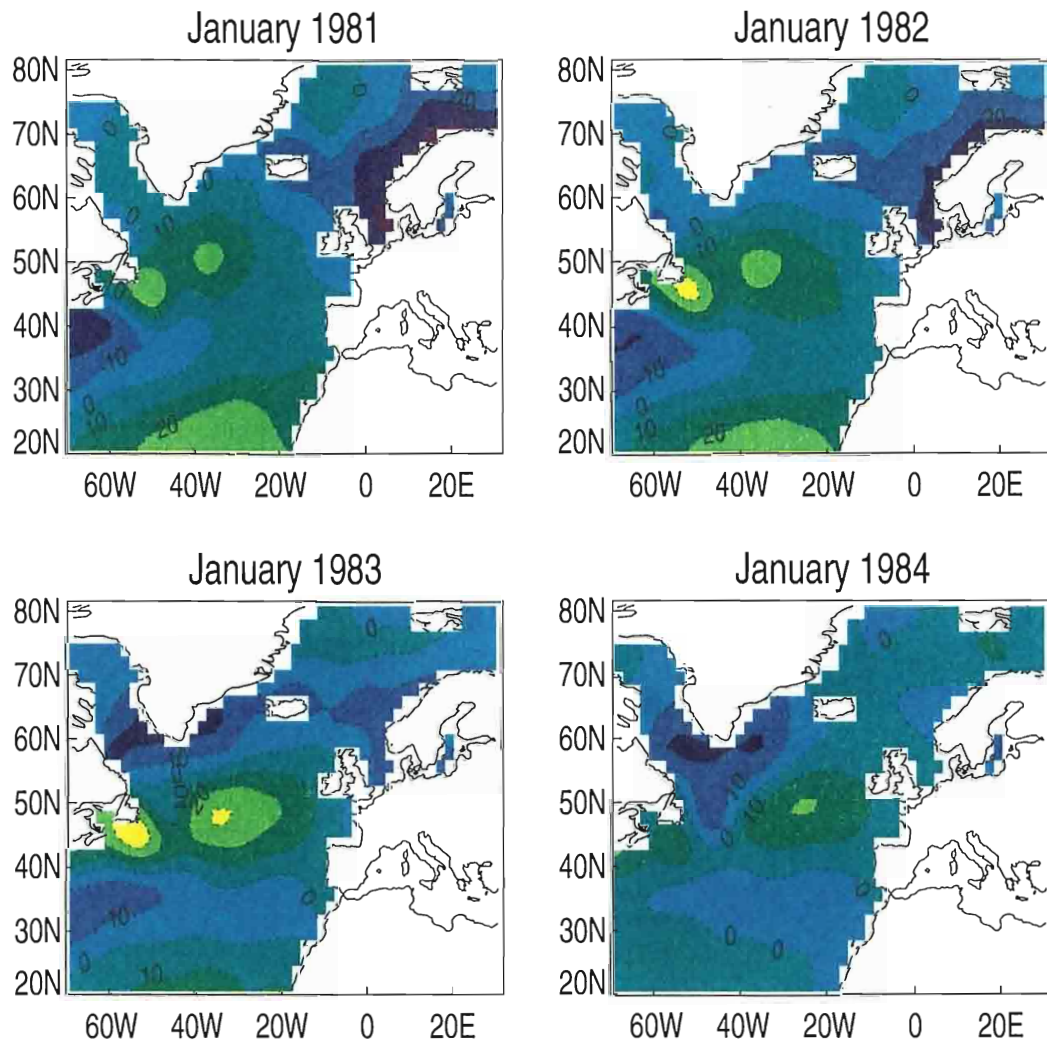# Chronology of SSTA (CEOF Mode2+3)

Figure 30: (continued)
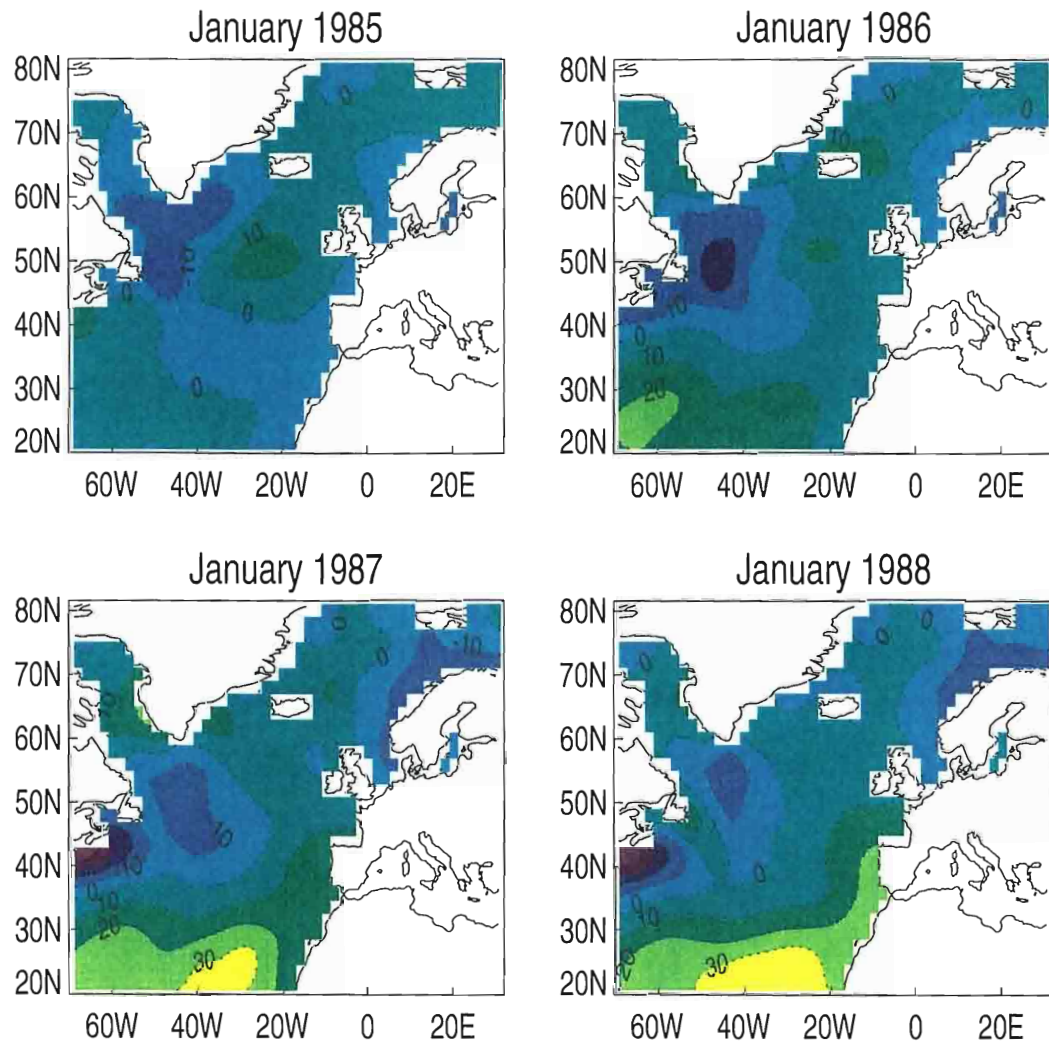
Chronology of SSTA (CEOF Mode2+3)

Figure 31:   (continued)
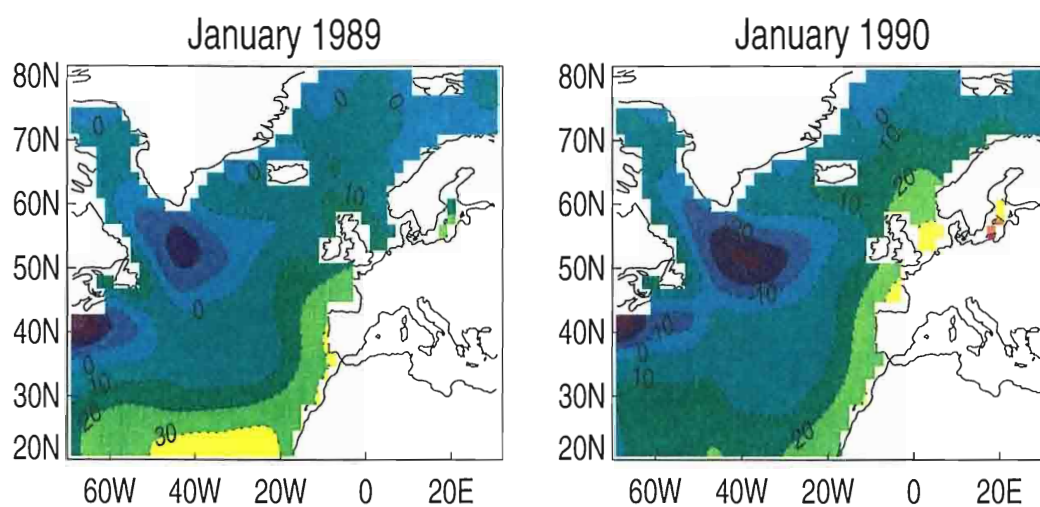
Chronology of SSTA (CEOF Mode2+3)
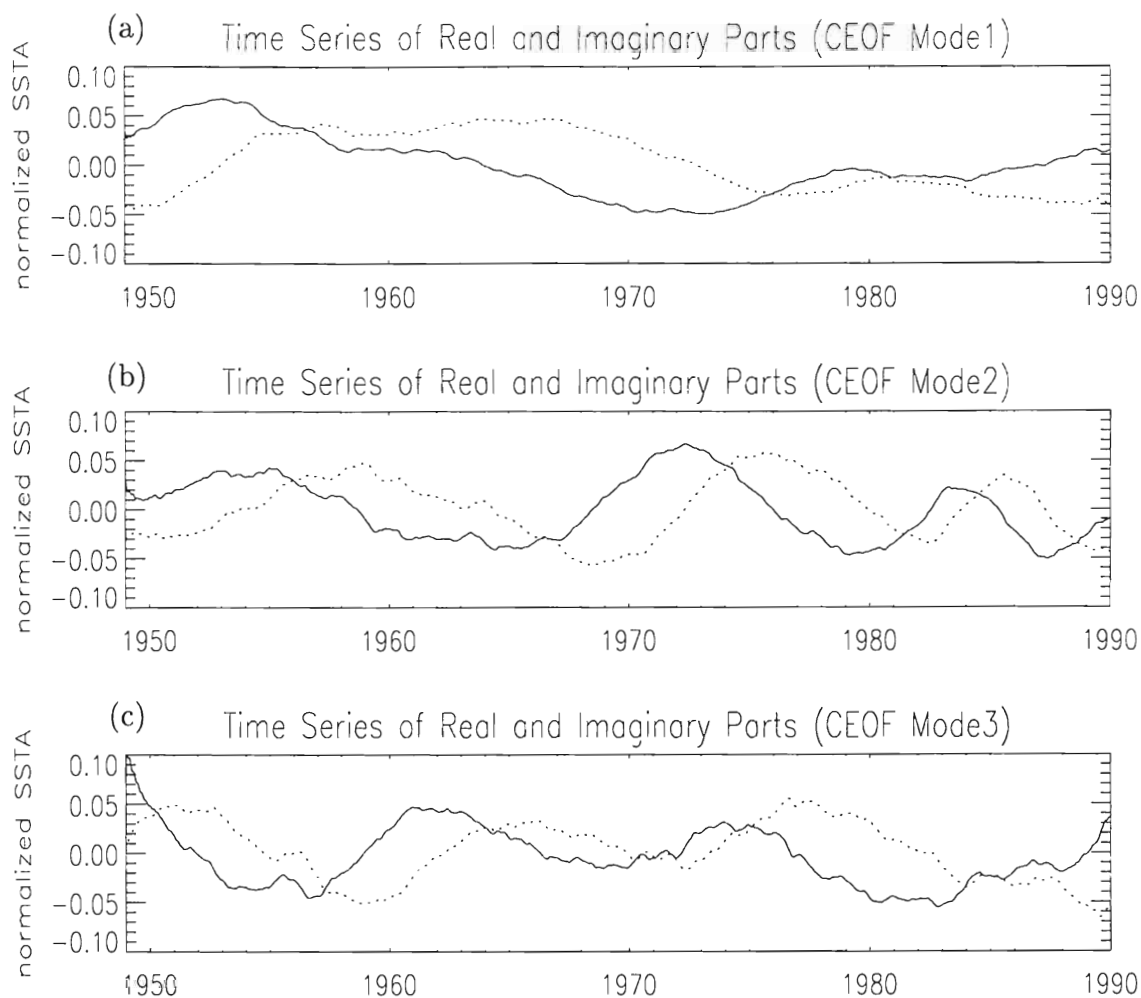

Figure 32: (continued)

Figure 33: Time series of real and imaginary parts of the temporal functions obtained from CEOF. (a), (b), (c) correspond to mode1, mode2 and mode3, respectively. Solid lines are real parts and dotted lines are imaginary parts. The y axis is normalized SSTA by dividing by 2 standard deviation.
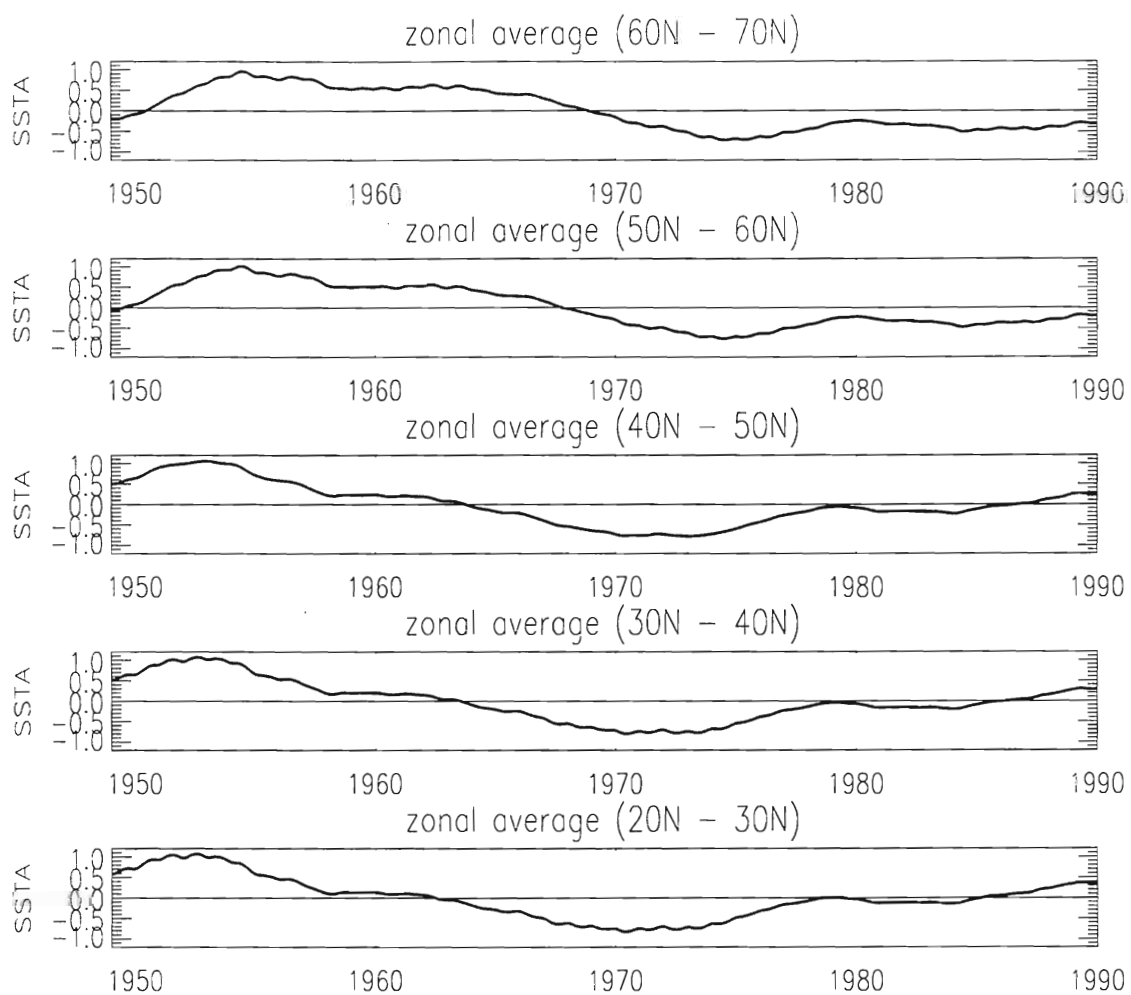
Figure 34: SSTA zonally-averaged in five 10° latitude belts between 20° N and 70° N. The y axis is normalized SSTA by dividing by 2 standard deviation.
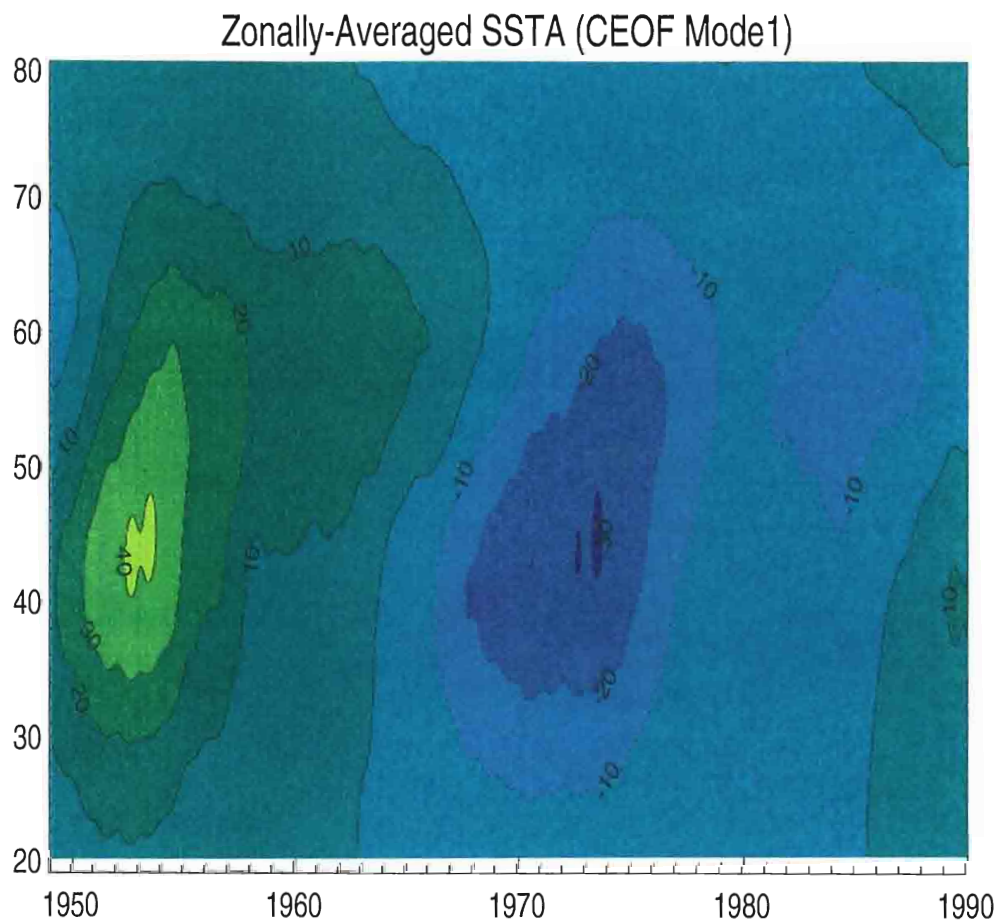
Figure 35: Time-latitude plot of SSTA obtained from CEOF mode1 and zonally averaged across the North Atlantic between 20° N and 80° N.
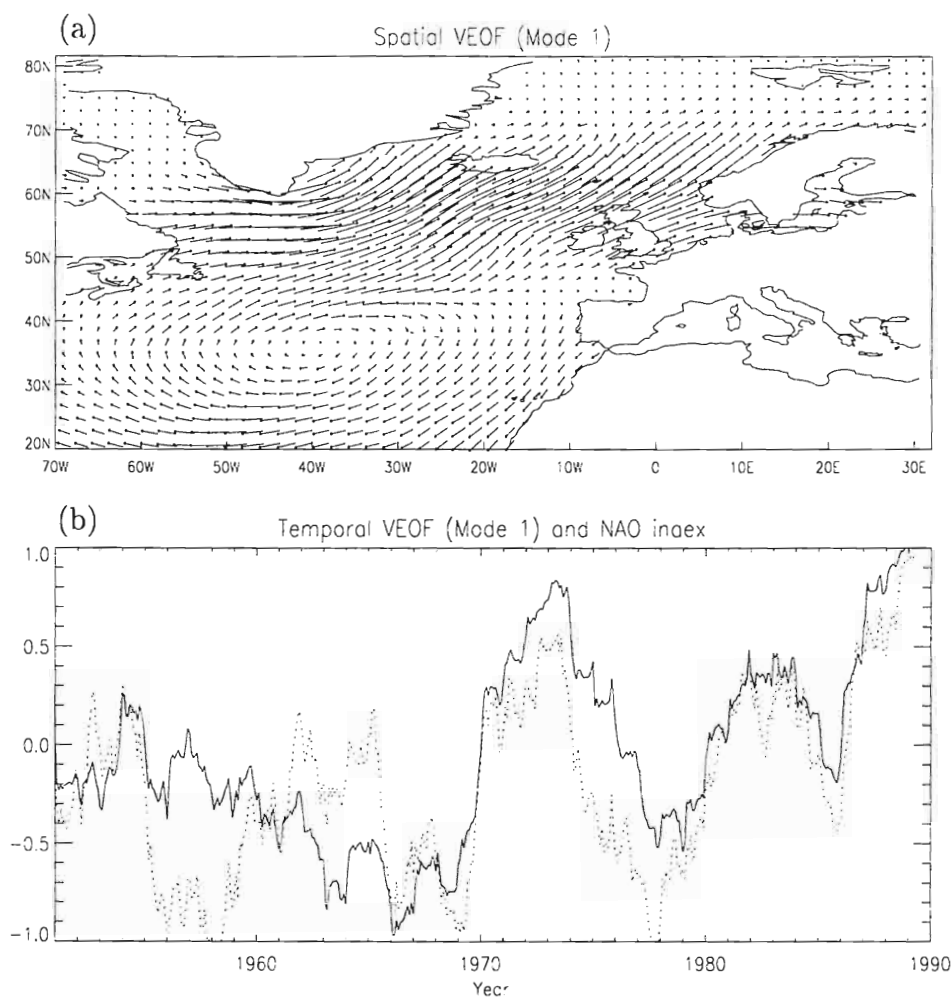
Figure 36: (a) Spatial and (b) temporal functions of Vector EOF analysis mode 1. (a) The vector field is in the positive phase of the NAO. (b) The solid line is the real part of the time function. Dotted line is NAO index after 4 year low-pass filtered. Correlation coefficient between the two time series is $r=0.79$ at 0 lag.

Time Series of SST Anomalies and VEOF1

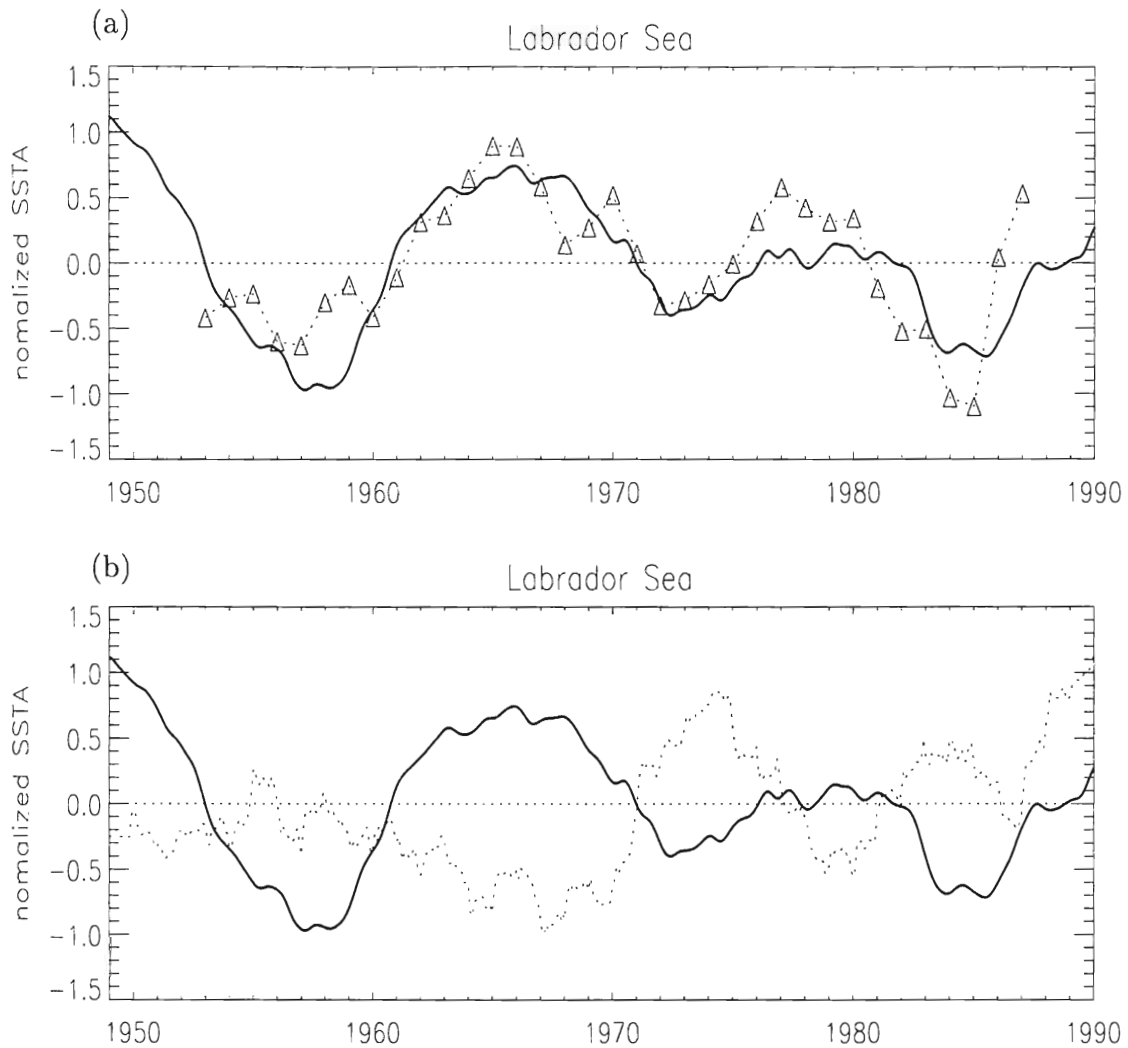Figure 37: SSTA time series in Labrador Sea region. (a) Time series from CEOF mode2+3. Dotted line is SSTA time series from Houghton (1996). (b) The dotted line is the time series of windstress from Vector EOF analysis. This is the real part of the time function when North Atlantic Oscillation (NAO) is in the positive phase. All the time series are normalized by dividing by 2 standard deviation.

64

(a)

(b)

(c)
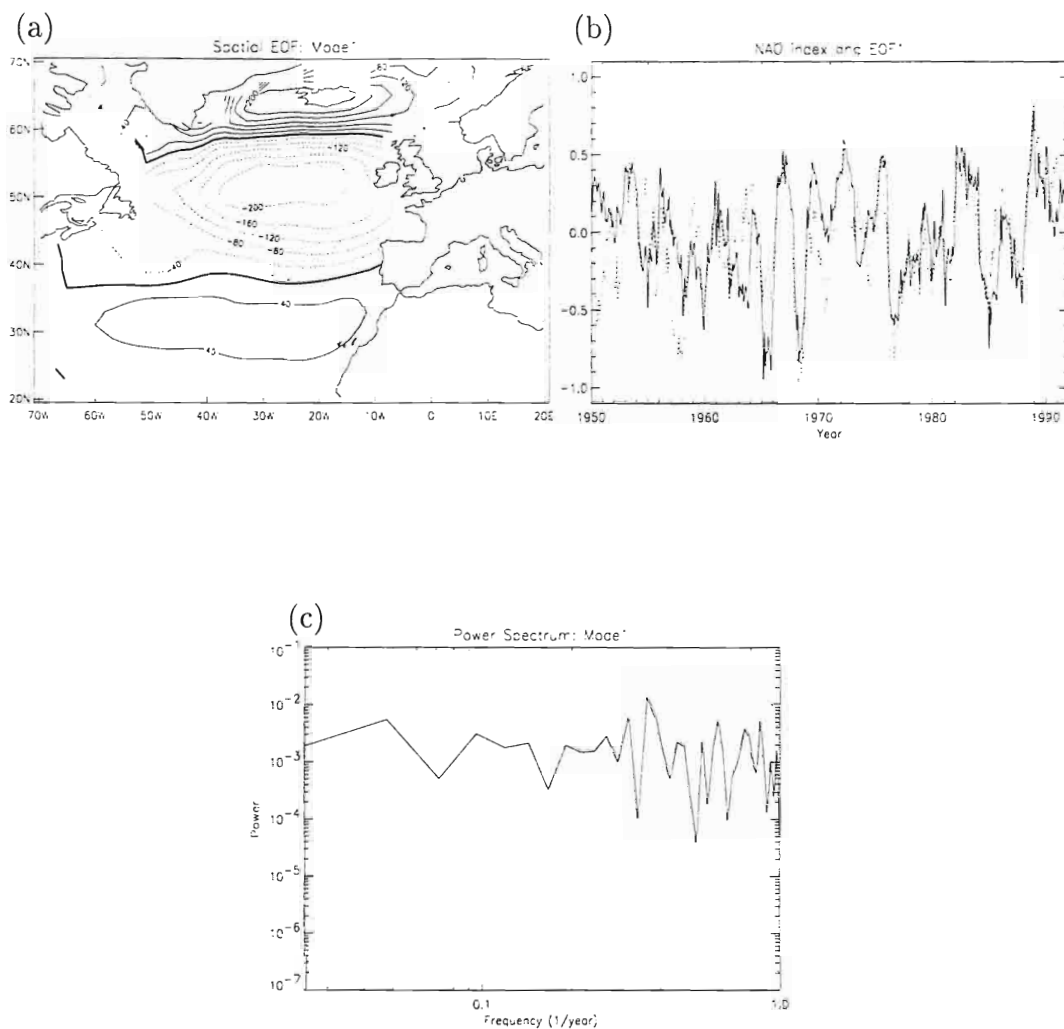
Figure 38:   (a) Spatial and (b) temporal EOF1 of pseudo stress curl, calculated from the data with the climatology removed. It explains 18.7% of the total variance. Units are $m\ s^{-2} \times 10^{-5}$. Contour intervals are $40ms^{-2} \times 10^{-5}$. Solid line is normalized time series associated with EOF1. Superimposed is the time series of NAO index as in Fig. 1. Both time series are low-pass filtered($>$12 months).

(a) Spatial EOF: Mode2

(b) EOF2

(c) Power Spectrum : mode 2

Figure 39:   Same as Fig. 38 except for EOF2. It explains 14.8% of the total variance.

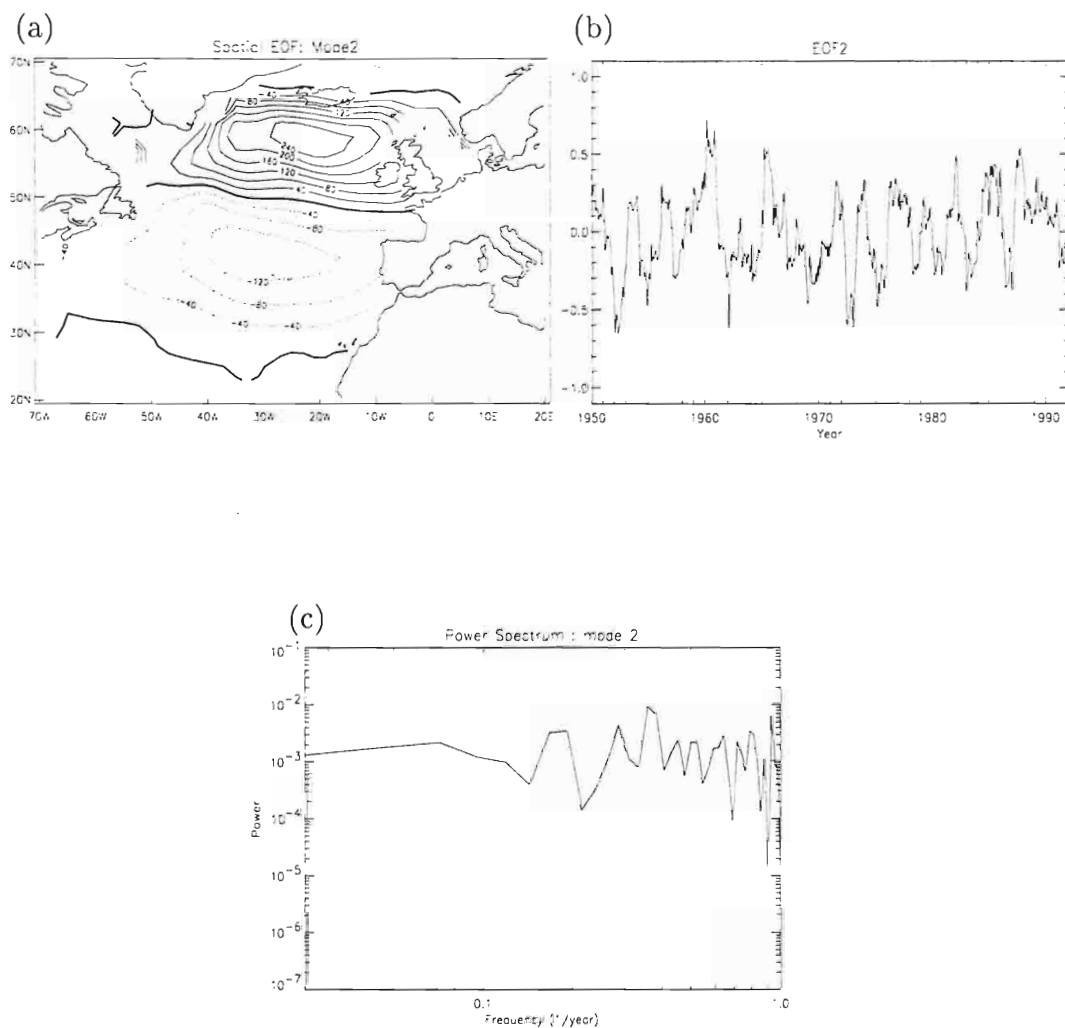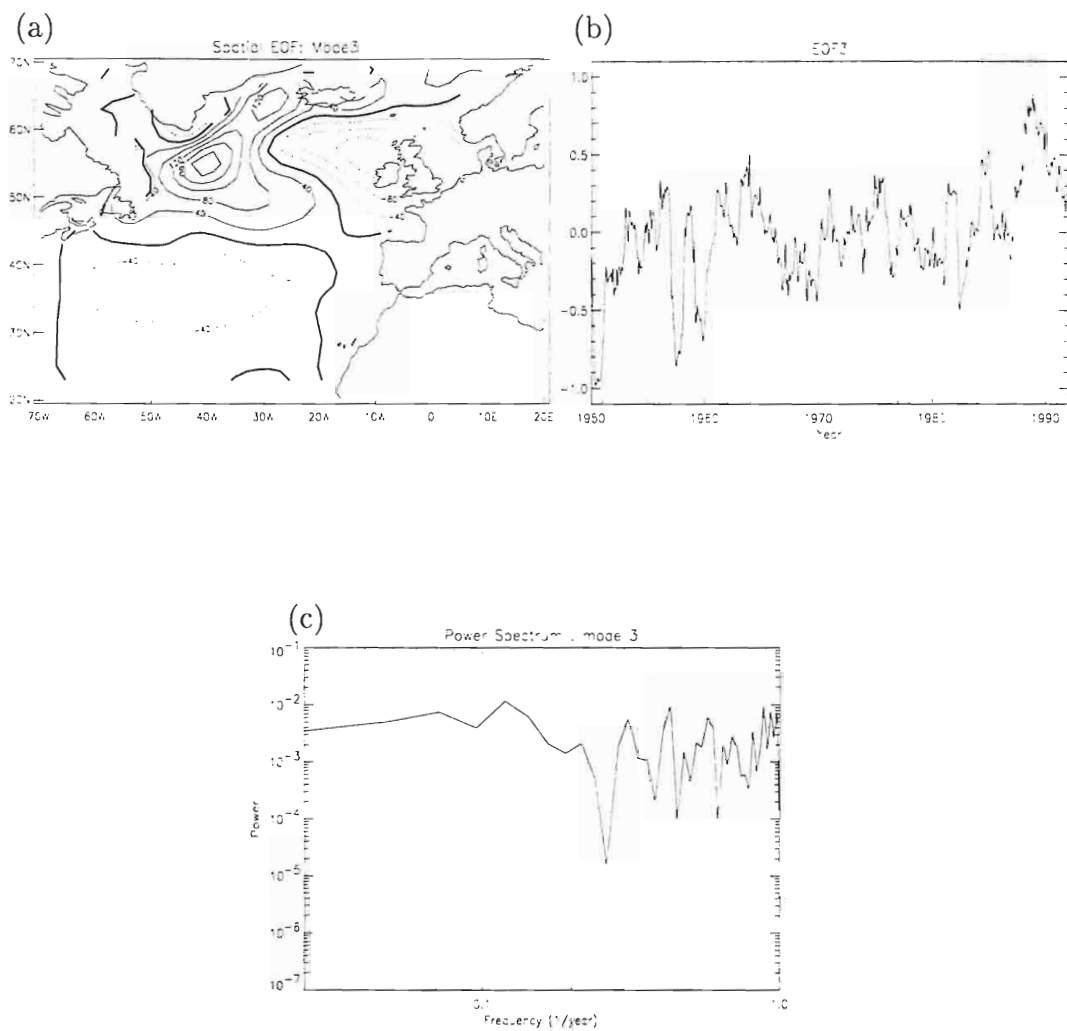Figure 40: Same as Fig. 38 except for EOF3. It explains 6.0% of the total variance.
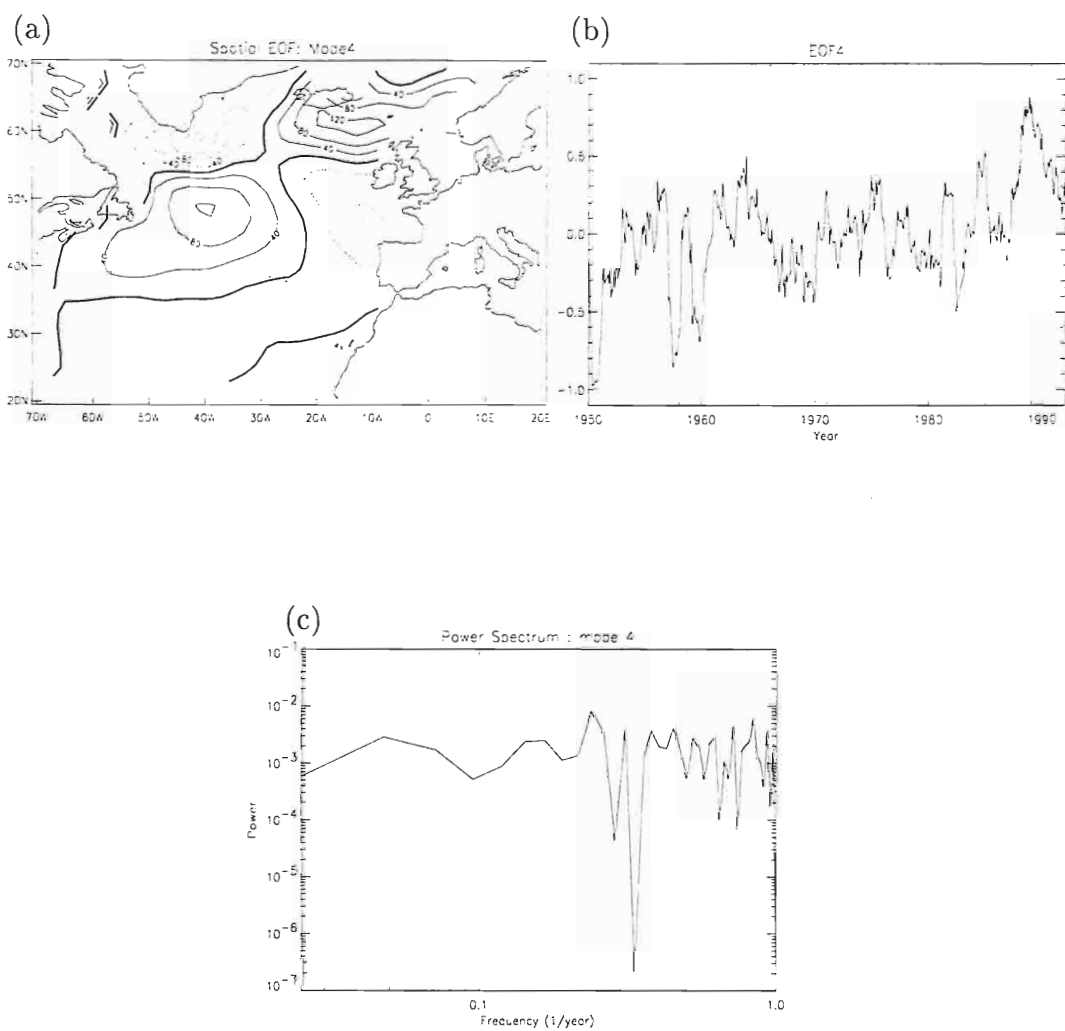
(a) Spatial EOF: Mode4

(b) EOF4

(c) Power Spectrum : mode 4

Figure 41: Same as Fig. 38 except for EOF4. It explains 4.8% of the total variance.

68

References

Barnett, T. P., 1983: Interaction of the Monsoon and Pacific Trade Wind System at Interannual Time Scales. Part I: The Equatorial Zone. Mon. Wea. Rev., **111**, 756–773.

Barnston, A. G., 1987: Classification, Seasonality and Persistence of Low-Frequency Atmospheric Circulation Pattern. Mon. Wea. Rev., **115**, 1083–1126.

Belkin, I., S. Levitus and J. Antonov, 1996: On the North Atlantic "Great Salinity Anomaly" of the 1980s. Submitted to Prog. Oceanog.

Bjerknes, J., 1964: Atlantic air-sea interaction. Advances in Geophysics. Academic Press, pp. 1–82.

Breidenbach, J., 1990: EOFs of Pseudo-Stress over the Indian Ocean (1977-85). Bull. Amer. Meteor. Soc., **71**, 1448–1454.

Cayan, D. R., 1992a: Latent and Sensible Heat Flux Anomalies over the North Oceans: Driving the Sea Surface Temperature. J. Phys. Oceanogr., **22**, 859–881.

Cayan, D. R., 1992b: Latent and Sensible Heat Flux Anomalies over the North Oceans: The Connection to Monthly Atmospheric Circulation. J. Clim., **5**, 354–369.

Delworth, T., S. Manabe and R. J. Stouffer, 1993: Interdecadal Variations of the Thermohaline Circulation in a Coupled-Atmosphere Model. J. Clim., **6**, 1993–2011.

Deser, C. and M. L. Blackmon, 1993: Surface Climate Variations over the North Atlantic Ocean during Winter: 1900-1989. J. Clim., **6**, 1743–1353.

Dickson, R. R., J. Lazier, J. Meincke, P. Rhines and J. Swift, 1996: Long-term coordinated changes in the convective activity of the North Atlantic. accepeted Prog. Oceanog.

Dickson, R. R., J. Meincke, S.-A. Malmberg and A. J. Lee, 1988: The "Great Salinity Anomaly" in the Northern North Atlantic 1968-1982. Prog. Oceanog., **20**, 103–151.

Frankignoul, C., P. Muller and E. Zorita, 1997: A Simple Model of the Decadal Response of the Ocean to Stochastic Wind Forcing. J. Phys. Oceanogr., **27**, 1533–1546.

Grötzner, A., M. Latif and T. P. Barnett, 1996: A decadal climate cycle in the North Atlantic Ocean as simulated by the ECHO coupled GCM. Submitted to Journal of Climate.

Häkkinen, S., 1993: An Arctic Source for the Great Salinity Anomaly: A Simulation of the Arctic Ice-Ocean System for 1955-1975. J. Geophy. Res., **98**, **C9**, 16,397–16,410.

Hansen, D. V. and H. F. Bezdek, 1996: On the nature of decadal anomalies

in North Atlantic sea surface temperature. J. Geophy. Res., **101, C4,** 8749–8758.

Horel, J., 1984: Complex principal component analysis: Theory and examples. J. Climate Appl. Meteor., **23**, 1660–1673.

Houghton, R. W., 1996: Surface Quasi-Decadal Fluctuations in the North Atlantic. J. Clim., **9**, 1363–1373.

Kushnir, Y., 1994: Interdecadal Variations in North Atlantic Sea Surface Temperature and Associated Atmospheric Conditions. J. Clim., **7**, 141–157.

Latif, M. and T. P. Barnet, 1994: Cause of Decadal Climate Variability over the North Pacific and North America. Science, **266, 28 Oct.,** 634–637.

Lazier, J. R. N., 1980: Oceanographic conditions at Ocean Weather Ship Bravo, 1964-1986. Atmos. Ocean., **18**, 227–238.

Legler, D. M., 1983: Empirical Orthogonal Function Analysis of Wind Vectors over the Tropical Pacific Region. Bull. Amer. Meteor. Soc., **64**, 234–241.

Lozier, M. S., W. B. Owens and R. G. Curry, 1995: The Climatology of the North Atlantic. Prog. Oceanog., **36**, 1–44.

Mauritzen, C. and S. Häkkinen, 1997. Submitted to JPO.

McCartney, M. S. and L. D. Talley, 1982: The subpolar mode water of the North Atlantic Ocean. J. Phys. Oceanogr., **12**, 1169–1188.

71

Molinari, R. L., D. A. Mayer, J. F. Festa and H. F. Bezdek, 1997: Multiyear variability in the near-surface temperature structure of the midlatitude western North Atlantic Ocean. J. Geophy. Res., **102, C2**, 3267–3278.

Reverdin, G., D. Cayan and Y. Kushnir, 1997: Decadal variability of hydrography in the upper northern North Atlantic in 1948-1990. J. Geophy. Res., **102, C4**, 8505–8531.

Rogers, J. C. and H. V. Loon, 1978: The seasaw in winter temperatures between Greenland and Northern Europe. part I:General Description. Mon. Wea. Rev., **106**, 296–310.

Rogers, J. C. and H. V. Loon, 1979: The seesaw in winter temperatures between Greenland and Northern Europe. PartII: some oceanic and atmospheric effects in middle and high latitudes. Mon. Wea. Rev., **107**, 509–519.

Schmitt, R. W., 1996: Oceanus. Vol. 39, 2.

Servain, J. and D. M. Legler, 1986: Empirical orthogonal function analyses of Tropical Atlantic sea surface temperature and wind stress: 1964-1979. J. Geophy. Res., **91(C12)**, 14181–14191.

Sharp, R. J., 1996: Complex Empirical Orthogonal Function Analysis in Two Dimensional Data Sets: Theory and Examples. Bachelors Thesis at Florida State University.

Shriver, J. F., M. A. Johnson and J. J. O'Brien, 1991: Analysis of Remotely Forced Oceanic Rossby Waves off California. J. Geophy. Res., **96, C1**, 749–757.

Talley, L. D., 1984: Meridional heat transport in the Pacific Ocean. J. Phys. Oceanogr., **12**, 1189–1205.

Wallace, J. M. and D. S. Gützler, 1981: Teleconnections in the geopotential height field during the northern hemisphere winter. Mon. Wea. Rev., **109**, 784–812.

Weaver, A. J. and E. S. Sarachik, 1991: Evidence for decadal variability in an ocean general circulation model: An advective mechanism. Atmos. Ocean, **29(2)**, 197–231.

Woodruff, S. D., R. J. Slutz, R. L. Jenne and P. M. Steurer, 1987: A comprehensive ocean-atmosphere data set. Bull. Amer. Meteor. Soc., **68**, 1239–1250.

BIOGRAPHICAL SKETCH

Degrees

B.E. 1992, Kagoshima University (Japan)

M.S. 1994, Kyushu University (Japan)

Memberships

Member of American Geophysical Union

Member of American Meteorological Society